

**CO GAS SENSOR APPLICATIONS OF Fe DOPED
CALIX[4]ARENE MOLECULES**

**A Thesis submitted to
the Graduate School of Engineering and Sciences of
İzmir Institute of Technology
in Partial Fulfilment of the Requirements for the Degree of**

MASTER OF SCIENCE

in Physics

**by
Cebraıl ÖZBEK**

**July 2013
İZMİR**

We approve the thesis of **Cebrail ÖZBEK**

Examining Committee Members:

Assoc. Prof. Gülnur AYGÜN ÖZYÜZER
Department of Physics, Izmir Institute of Technology

Prof. Dr. Salih OKUR
Department of Material Science and Engineering, Izmir Katip Celebi University

Prof. Dr. Lütü ÖZYÜZER
Department of Physics, Izmir Institute of Technology

Assist. Prof. Ömer MERMER
Department of Electrical-Electronics Engineering, Gediz University

Assist. Prof. Enver TARHAN
Department of Physics, Izmir Institute of Technology

5 July 2013

Assoc. Prof. Gülnur Aygün ÖZYÜZER
Supervisor, Department of Physics,
Izmir Institute of Technology

Prof. Dr. Salih OKUR
Co-Supervisor, Department of
Material Science and Engineering,
Izmir Katip Celebi University

Prof. Dr. Nejat BULUT
Head of the Department of Physics

Prof. Dr. R. Tugrul SENGER
Dean of the Graduate School of
Engineering and Sciences

ACKNOWLEDGEMENTS

Firstly, I would like to thank my co-advisor, Dr. Salih Okur. His encouragement and support made this thesis possible. He was actually my advisor but since he moved to Izmir Katip Celebi University he had to be my co-advisor due to regulations. I also would like to thank Prof. Dr Mustafa Yılmaz, Serkan Sayın and his research group in Selçuk University, Assist. Prof Dr Ömer Mermer from Ege University, Prof Dr Mustafa Kurt from Ahi Evran University and Mustafa Can from İzmir Katip Çelebi University for their contribution to this thesis. I would like to thank Applied Quantum Research Center at Iztech. I used clean room and infrastructure of it. This thesis was supported by TUBITAK under project number 109T240. I also would like to thank to my Advisor Assoc. Prof Gulnur Aygun Ozyuzer. Moreover, I want to thank to my lab mates, Hasan Aydin, Abdullah Bayram, Halis Guzelaydin, Cem Baytore, Nesli Yağmurcukardeş, and Fevzi Sümer for providing a wonderful working environment. Of course, Fevzi and Abdullah deserve my special thanks for their friendship, supporting and discussing with my experimental work.

Finally, I can't find better words to explain contribution of my family to my education and explain their love. I express my thanks for their helps.

ABSTRACT

CO GAS SENSOR APPLICATIONS OF Fe DOPED CALIXARENE MOLECULES

Invisible and odourless carbon monoxide (CO) is one of the most toxic gas for respiratory systems. Therefore, the concentration level of carbon monoxide in the environment is extremely vital. In this thesis study, Calixarene molecules have been synthesized and the carbon monoxide selectivity and sensitivity of bare and iron doped calixarene molecules were measured by quartz crystal microbalance QCM technique and interdigitated electrodes with 3 μm spacing.

Calixarenes are promising compounds for sensing studies due to the well-designed cyclic structure, easily derivatization at both *p*- position of phenolic ring (*upper rim*) and phenolic-O (*lower rim*) as well as having diversely cavities which are a straightforward platform to form complex with molecules and ions. Quartz Crystal Microbalance is a powerful technique for nano scale determining the sorption properties of materials. According to Sauerbrey relation, the mass change on quartz crystal electrode cause a certain shift in the resonant frequency of vibrating crystal oscillator. This shift can be monitored using QCM method.

In this study, a computer controlled QCM measurement system was developed for toxic gas detection. Iron doped calixarene based sensors were fabricated using drop-casting method on an AT-cut QCM gold electrode and interdigitated gold electrodes. The sensitivity and reproducible detection performances of prepared calixarene-iron doped calixarene thin films were measured under exposure of varying carbon monoxide for nitrogen and dry air used as desorption gas, respectively.

The analysis of carbon monoxide sensitivity of iron doped calixarene is a new study for literature. This thesis study will guide future studies on this topic.

ÖZET

DEMİR KATKILI KALİKSAREN MOLEKÜLLERİNİN CO GAZ SENSÖR UYGULAMALARI

Renksiz ve kokusuz karbon monoksit (CO) gazı bilindiği üzere canlılar için ölümcül gazlardan birisidir. Bu yüzden ortamdaki CO konsantrasyonunu ölçmek son derece hayati bir durumdur. Bu tez çalışmasında demir molekülleri ile katkılanmış kaliksaren moleküllerinin karbon monoksit gazına olan hassasiyeti ve seçiciliği, kuartz kristal mikrobalsan tekniği ile araştırılmasının yanı sıra, iç içe geçmiş taraklı elektrotlar (İTE) üzerinde oluşturulan ince filmlerin elektriksel özelliklerindeki değişime bağlı olarak incelenmiştir.

Kaliksarenler, halkalı yapıda olması, kolaylıkla hem fenolik halkaların *p*-pozisyonundan (*upper rim*) hem de fenolik-O kısımlarından (*lower rim*) türevlendirilebilmesinin yanında molekül ve iyonlarla kolay kompleks yapabilmelerini sağlayan farklı halka boşluklarının olması nedeniyle sensör çalışmaları için uygun bileşiklerdir.

Kuartz kristal mikrobalsan, nanogram mertebesinde, malzemelerin gaz tutma özelliklerini inceleyebileceğimiz bir tekniktir. Sauerbrey ilişkisine göre, kristal elektrotundaki kütle değişimi, titreşen kristal elektrotta belirli bir frekans kaymasına neden olur. Bu değişim QCM metodu ile ölçülebilir.

Kuartz kristal mikrobalsan metodunun kullanıldığı bu tez çalışmasında bilgisayar kontrollü gaz akış ve gaz karışım sistemi ile nanogram mertebesinde algılayıcı malzemelerin zehirli gaz tutma özelliklerinin incelenebileceği deneysel düzenek tasarlanmıştır. AT-kesim QCM altın elektrotlar ve iç içe geçmiş taraklı elektrotlar demir katkılı kaliksarenler ve normal kaliksarenler ile damlatma metodu kullanılarak kaplanmıştır. Hazırlanan kaliksaren-demir katkılı kaliksaren ince filmleri değişen karbon monoksit konsantrasyon oranlarına maruz bırakılarak hassasiyetleri ve tekrarlanabilir algılama performansları, desorpsiyon amacıyla kullanılan yüksek saflıkta azot ve kuru hava için ölçülmüştür.

Farklı fonksiyonel gruplara sahip kaliksaren moleküllerinin demir ile katılanıp karbon monoksit gazına karşı hassasiyetlerini incelemek literatürde rastlanmamış bir çalışmadır. Bu tez, bu anlamda ileriki çalışmalara temel teşkil ederek yön vereceği kesindir.

To my Family

TABLE OF CONTENTS

LIST OF FIGURES	viii
LIST OF TABLES	x
CHAPTER 1. INTRODUCTION.....	1
CHAPTER 2. GAS SENSORS	5
2.1.Characteristics for an ideal sensor	8
2.2.Types of Gas Sensors.....	11
2.2.1.Semiconductor gas sensors	12
2.2.2.Field Effect Transistor (FET) gas sensors	13
2.2.3.Optical Gas Sensors	14
2.2.4.Electrochemical gas sensors	15
2.2.5.Catalytic Gas Sensors	16
2.2.6.Piezoelectric gas sensors.....	17
2.3.Theoretical Foundations	18
2.3.1.Piezoelectric effect and principle of QCM	18
2.4.Calixarenes.....	25
CHAPTER 3. EXPERIMENTAL DETAILS	32
3.1.Gas flow control and measurement system	32
3.2.Device Fabrication (IDE): Photolithography technique	37
3.3.Iron doping procedure of various functional calixarene molecules and preparation of QCM electrodes	43
CHAPTER 4. RESULTS AND DISCUSSIONS	49
4.1.Investigation of CO gas sorption kinetics of molecules using QCM method	49
4.1.1.Investigation of CO gas sorption kinetics of all calixarene molecules using QCM method	52
4.1.2.Investigation of adsorption and desorption of all molecules with Langmuir adsorption model	69
4.2.Electrical Results	76
CHAPTER 5. CONCLUSION	81
REFERENCES	84

LIST OF FIGURES

<u>Figure</u>	<u>Page</u>
Figure 1.1. Calixarenes with different ring number.....	3
Figure 2.1. Signal processing in living organisms and intelligent machines.....	6
Figure 2.2. Scheme of a typical chemical sensor.....	7
Figure 2.3. Examples of accuracy and precision	9
Figure 2.4. Dependence of signal generated by sensor on concentration.....	10
Figure 2.5. Example of interference in gas sensors	10
Figure 2.6. Basic components of metal oxide based semiconductor gas sensor.....	13
Figure 2.7. Basic structure of FETs	13
Figure 2.8. Optical apparatus used for NO ₂ gas sensing application.....	14
Figure 2.9. Basic electrochemical gas sensor (left) and typical electrochemical gas sensor with three electrodes design (right)	16
Figure 2.10. Basic structure of a SAW device.....	17
Figure 2.11. Pure Quartz crystal and different quartz crystal cuts	20
Figure 2.12. AT-cut and BT-cut crystals	20
Figure 2.13. AT-cut angle of quartz crystal and natural vibration frequency, temperature and cut angle dependence of quartz crystal	21
Figure 2.14. Cross-sectional and surface-view of a quartz crystal microbalance.....	22
Figure 2.15. General structure of calix[4]arene	26
Figure 2.16. Different conformations of p-tert-butyl calixarene	27
Figure 2.17. Host-guest interactions in supramolecular systems.....	28
Figure 2.18. Calixarenes used as NO ₂ sensor	29
Figure 2.19. Acoustic wave sensor based on calixarenes	29
Figure 2.20. Calixarene molecules synthesized to detect volatile organic compounds..	30
Figure 2.21. Humidity sensing properties of a sulphonate calixarene derivative.....	31
Figure 3.1. Schematic of gas flow system	33
Figure 3.2. CHI400A EQCM.....	34
Figure 3.3. Coated and uncoated QCM electrodes	34
Figure 3.4. MKS 179A Mass-Flo® flow meters	35
Figure 3.5. MKS 647C and Keithley 2636A Sourcemeter	35
Figure 3.6. The box including test cell and the whole experimental setup.....	36
Figure 3.7. Schematic of plasma cleaning procedure	37
Figure 3.8. (a) and (b) Evaporation system with plasma cleaning option (c) during plasma cleaning (d) schematic of evaporation.....	38
Figure 3.9. Class 1000 clean room	39
Figure 3.10. Photolithography steps. (1) cleaning, (2) Cr film deposition, (3) Au film deposition, (4) positive resist coating, (5) UV light exposure, (6)development, (7) Au etching, (8) Cr etching	40
Figure 3.11. (a) Hot plate, (b) spin coater, (c) mask aligner and (d) mask.....	41
Figure 3.12. Mask design used to expose positive photoresist.....	42

Figure 3.13. Aqua regia (Au etchant), (b) Cr etchant	42
Figure 3.14. Bare calixarene, Fe(1) doped calixarene, Fe(2) doped calixarene	47
Figure 3.15. Cleaning of QCM electrodes	48
Figure 3.16. Preparation of thin films on QCM using drop-casting technique	48
Figure 4.1. Steps of periodic measurement.....	50
Figure 4.2. Steps of linear measurement.....	51
Figure 4.3. Periodic responses of all various functional calixarene molecules to CO ...	55
Figure 4.4. Periodic responses of Fe(1) doped calixarene molecules to CO	57
Figure 4.5. Periodic responses of Fe(2) doped calixarene molecules to CO	58
Figure 4.6. Bar graphs illustrating maximum responses of all molecules to CO	59
Figure 4.7. Sensitivities of bare calixarenes to CO.....	61
Figure 4.8. Sensitivities of Fe(1) doped calixarenes to CO	62
Figure 4.9. Sensitivities of Fe(2) doped calixarenes to CO	63
Figure 4.10. Bar graph showing maximum sensitivities of all molecules.....	65
Figure 4.11. Linear responses of bare calixarenes to CO	65
Figure 4.12. Linear responses of Fe(1) doped calixarenes to CO.....	66
Figure 4.13. Linear responses of Fe(2) doped calixarenes to CO.....	66
Figure 4.14. CO sensitivities of bare calixarenes in air environment.....	67
Figure 4.15. sensitivities of Fe(1) doped calixarenes in air environment.....	67
Figure 4.16. sensitivities of Fe(2) doped calixarenes in air environment.....	68
Figure 4.17. Adsorbed mass on the surface of bare calixarene molecules versus time..	71
Figure 4.18. Adsorbed mass on the surface of Fe(1) doped calixarene molecules versus time	72
Figure 4.19. Adsorbed mass on the surface of Fe(2) doped calixarene molecules versus time	72
Figure 4.20. QCM results of bare calixarenes: the least square fit (solid lines) using the Langmuir adsorption isotherm model given in Equation (5) for 10000 ppm CO concentration.....	73
Figure 4.21. QCM results of Fe(1) doped calixarenes: the least square fit (solid lines) using the Langmuir adsorption isotherm model given in Equation (5) for 10000 ppm CO concentration.....	74
Figure 4.22. QCM results of Fe(2) doped calixarenes: the least square fit (solid lines) using the Langmuir adsorption isotherm model given in Equation (5) for 10000 ppm CO concentration.....	75
Figure 4.23. Steps of periodic measurement.....	77
Figure 4.24. Electrical response of Calix 8 under exposure of CO	78
Figure 4.25. Electrical response of CNT added Calix 6_Fe(2)	79
Figure 4.26. Sensitivity of CNT added Calix 6_Fe(2).....	80

LIST OF TABLES

<u>Table</u>	<u>Page</u>
Table 1.1. Symptoms according to CO concentration level	2
Table 2.1. The basic physical and chemical principles used by the sensor devices	8
Table 2.2. Types of solid state gas sensors with the corresponding physical change used as gas detection principle	12
Table 3.1. The parameter values used in photolithography process	43
Table 3.2. Molecular structures and chemical names of each calixarene molecule used in this thesis.....	44
Table 3.3 (cont.).....	45
Table 4.1. Molecular structure and three dimensional structure of calixarene molecules.....	53
Table 4.2 (cont.).....	54
Table 4.3. Dipole moments of calixarene molecules.....	54
Table 4.4. Maximum response of each undoped calixarene molecules to CO.....	56
Table 4.5. Maximum responses of Fe(1) doped calixarene molecules to CO	57
Table 4.6. Maximum responses of Fe(2) doped calixarene molecules to CO	58
Table 4.7. ΔF_o and Δm_o (μg) values of all molecules	60
Table 4.8. Maximum sensitivities of each undoped calixarene molecules to CO	61
Table 4.9. Maximum sensitivities of each Fe(1) doped calixarene molecules to CO	63
Table 4.10. Maximum sensitivities of each Fe(2) doped calixarene molecules to CO ..	64
Table 4.11. Maximum responses of all molecules in both air and N ₂ environment.....	68
Table 4.12. Langmuir fit results.....	76

CHAPTER 1

INTRODUCTION

As a product of the incomplete combustion of hydrocarbons, carbon monoxide (CO) is one of the most dangerous gases for living things. Carbon monoxide exposure is still one of the leading causes of unintentional and suicidal poisonings, and it causes a large number of deaths annually in all over the world. In addition, carbon monoxide may be the cause of more than one-half of the fatal poisonings reported in many countries(Raub et al., 2000). The affinity of haemoglobin for carbon monoxide compared to oxygen is 200 to 250 times greater. Carbon monoxide forms carboxyhemoglobin (HbCO) in the blood when combining with haemoglobin. As a consequence of this, haemoglobin cannot release oxygen in tissues, effectively reducing the oxygen-carrying capacity of the blood, giving rise to hypoxia. When exposed to CO, the health effects may be the more subtle cardiovascular and neurobehavioral effects at low concentrations. However, it may even result in unconsciousness and death after acute or chronic exposure to high concentrations of CO(Rodkey et al., 1974). The symptoms during exposure of CO according to concentration level in parts per million are listed in Table 1.1(Goldstein, 2008; Struttman et al., 1998). Therefore, it is vital to know the concentration level of carbon monoxide in the environment.

Table 1.1. Symptoms according to CO concentration level

Concentrations	Symptoms
35 ppm (0.0035%)	Headache and dizziness within six to eight hours of constant exposure
100 ppm (0.01%)	Slight headache in two to three hours
200 ppm (0.02%)	Slight headache within two to three hours; loss of judgment
400 ppm (0.04%)	Frontal headache within one to two hours
800 ppm (0.08%)	Dizziness, nausea, and convulsions within 45 min; insensible within 2 hours
1,600 ppm (0.16%)	Headache, tachycardia, dizziness, and nausea within 20 min; death in less than 2 hours
3,200 ppm (0.32%)	Headache, dizziness and nausea in five to ten minutes. Death within 30 minutes.
6,400 ppm (0.64%)	Headache and dizziness in one to two minutes. Convulsions, respiratory arrest, and death in less than 20 minutes.
12,800 ppm (1.28%)	Unconsciousness after 2–3 breaths. Death in less than three minutes.

In 1959, physicist Richard Feynman suggested that it should be possible, in principle, to make nanoscale machines that "arrange the atoms the way we want", and do chemical synthesis by mechanical manipulation. He opened a new era at his talk, entitled "There's Plenty of Room at the Bottom", on what later became known as "nanotechnology". Today, however, research on producing more sensitive, cheaper and low-power gas sensors shows a great improvement in parallel with the rapid developments in the nanotechnology world. Nanomaterials, having very high surface-to-volume ratio as well as porous structure, are ideal for gas sensing applications with adsorbing capabilities of gas molecules. Hence, nanomaterial based gas sensor applications such as carbon nanotubes (CNT), nanowires, nanoparticles and nanofibres are being conducted.

Due to the excellent gas sorption capabilities, long time stable structure and suitable characteristics for technological applications, calixarene molecules, used in the thesis, are convenient compounds for sensor applications. Calixarenes, product of the condensation reaction of phenol with formaldehyde in the basic environment, are ring structured macro cyclic compounds. Unlimited ability of functionalization features and forming "host-guest" complexes enable these molecules to be used in selectivity and sensitivity applications. Varying the number of aryl fragments and functional groups it is easy to manage with sensitivity and selectivity of calixarene films. Chemical modification of calixarene represents an effective and versatile way of producing

receptors with highly selective binding properties(Kim and No, 2007). Calixarenes, known as macro cyclic compounds, are joined by methylene groups attached at positions ortho to the hydroxyl groups(Gutsche and Stoddart, 1989).

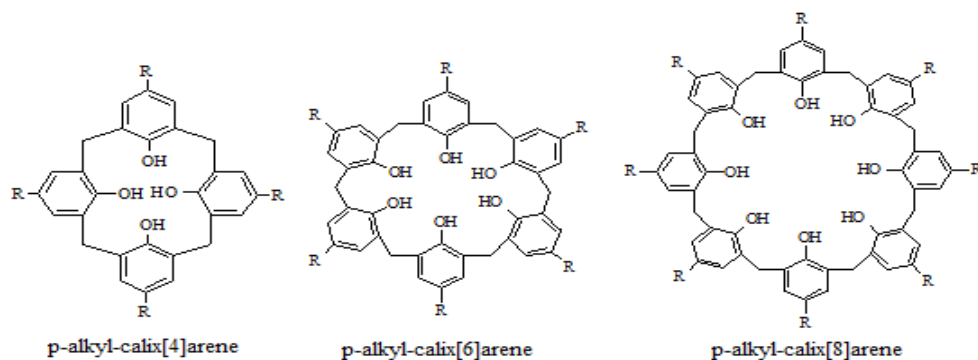


Figure 1.1. Calixarenes with different ring number

Calixarenes are considered to be convenient for CO gas sensor application in this thesis since they have cyclic structure and can easily be functionalized for any desired purpose as well as capable of forming annular gap in different size. Hence, various calixarene molecules having different functional groups, in particular those of which include amine, are synthesized so as to carry out this thesis study. In addition, gas sorption kinetics of the prepared composite compounds are investigated under exposure of different concentrations of CO gas. Composite thin film coated quartz crystal microbalance electrodes having piezoelectric nature and allowing to measure the frequency shift as a result of mass changes due to the adsorption and desorption of gas molecules were used as a research method in this study. Because QCM method has quite sensitive sensing capability of the order of nanograms, feasibility and stable operation in room conditions, it has been widely used in gas detection applications in recent years. QCM binding kinetics of specific calixarene molecules that have affinity towards CO gas molecules have not been investigated well. Fevzi Sumer studied adsorption and desorption kinetics of carbon nanotube modified with various calixarene molecules for CO gas sensor applications. However, the present study is the first study that investigates the sorption kinetics of iron doped calixarene molecules. The purpose of doping iron molecules into the calixarene molecules is to increase sensitivity of

prepared thin films towards CO gas molecules. Furthermore, the reason why calixarene molecules containing amine groups are preferred is that the acid-base reaction has been supposed to take place. The sensitivity and selectivity properties of both iron doped and undoped calixarene molecules to CO gas were investigated. Basically, different types of gas sensors and the main features of ideal gas sensors are discussed in the first part of this thesis work. In the second part, some information about quartz crystal microbalance, calixarenes used as sensing materials are given and in addition to this, theoretical calculations and gas sorption kinetics of these materials are discussed. In the third chapter, the equipment used to carry out experiments is introduced and fabrication of IDE electrodes, iron doping process of calixarene molecules, thin film preparation on QCM electrodes are explained in details. The experimental results and data are presented in the fourth chapter.

CHAPTER 2

GAS SENSORS

A sensor is a device that measures physical or chemical changes and converts it into an electrical signal which can be read by an electronic instrument. Due to the sensors which are used in many areas of our daily lives and one of the products of the revolution in microprocessor ensuing the technology that has rapidly been developing from the beginning of 20th century to the present day, machinery, equipment and other automation systems can be controlled smarter, more efficiently and more quickly. In addition, sensors have applications in many areas such as medical identification, environmental monitoring, automotive, industrial production and the defence industry. People mimic organisms living on the basis of sensors that can be defined as artificial sensory organs. To exemplify, when the smell receptors in the structure of the mucosa touch a smell in air environment, the receptor cells detect these odour molecules and transmit as electrical signals through neuronal cells. Neurons carry these odour signals to the brain and the mechanism of perception is completed after the brain responds to these signals. Even though live nose is superior to all other known odour and gas sensors in nature in terms of selectivity, it has some weak points such as detection capability and ability to learn, olfactory fatigue, detection ability of only water-or oil-soluble molecules are weak points. Gas sensors can be used when taking critical measurements in the environments in which these weaknesses are available. Like a sensory organ, gas sensors detect the molecules in the environment with a detection material and it is converted into a signal which is then delivered to a microprocessor (brain) with the help of amplifier and carrier circuit (neuron). This signal is evaluated here and presented as information to the user as given in Figure 2.1. The development of sensors in recent years has become even more important because of developing technology and the needs of the physical, chemical and biological detection.

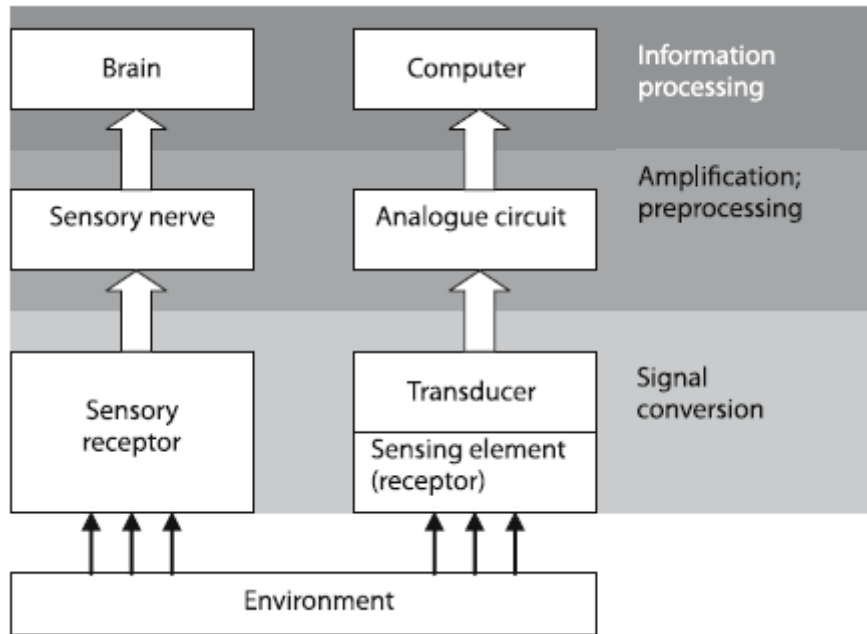


Figure 2.1. Signal processing in living organisms and intelligent machines

A sensor should;

- ✓ be directly in contact with the substance to be measured,
- ✓ convert non-electrical information into an electrical signal,
- ✓ be able to provide quick response,
- ✓ be stable and sustainable,
- ✓ be small,
- ✓ be producible and cheap(Gründler, 2007).

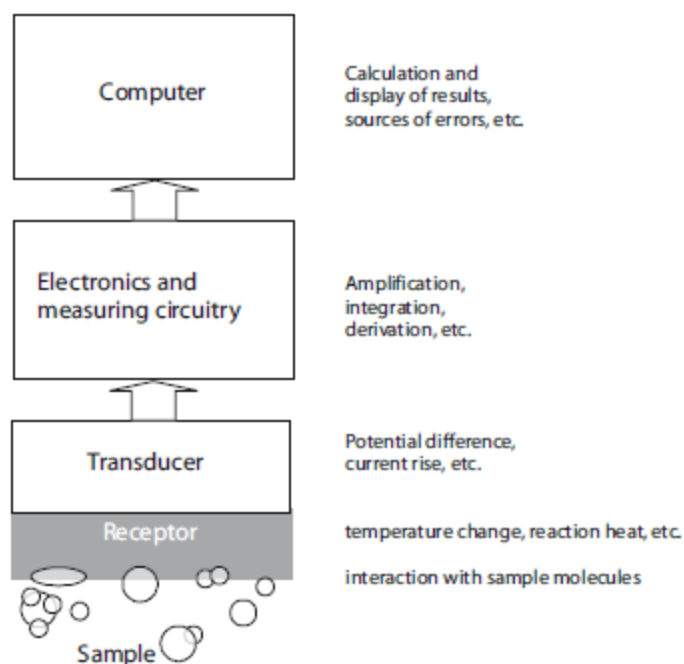


Figure 2.2. Scheme of a typical chemical sensor

Receptor systems in sensor systems are organic or inorganic sensitive materials obtained by various coating methods. Receptor materials, in contact with the external environment and interacting with the analyte molecules, are beginning parts of the sensing mechanism. Physical and chemical changes that result from the interaction of target analyte in environment with receptor material are transmitted to the transducer to be converted into electrical signal. A converter is a device that converts the energy to a different form of energy type. For example, the electrical energy in a fluorescent lamp is converted into light and heat energy. These energy types are based on chemical and physical based quantitative magnitudes. These magnitudes are classified as follows;

- ✓ Mechanical
- ✓ Thermal
- ✓ Electrical
- ✓ Magnetic
- ✓ Optical
- ✓ Chemical.

Examples for these magnitudes are presented in Table 2.1 for each class.

Table 2.1. The basic physical and chemical principles used by the sensor devices

	Quantity
Mechanical	Length, area, volume, velocity, acceleration, force, torque, pressure, sound wavelength, intensity etc.
Thermal	Temperature, heat, entropy, heat flow etc.
Electrical	Voltage, current, resistance, charge, inductance, capacitance, dielectric constant, polarization, electric field, frequency, dipole moment etc.
Magnetic	Flux density, magnetic moment, the magnetic permeability etc.
Optical	Intensity, phase shift, wavelength, polarization, refraction index etc.
Chemical	Concentration, reaction rate, pH, oxidation / reduction potentials etc.

As biosensors use biochemical process that is the source of the analytical signal, they may be considered as a specific type of chemical sensors(Hulanicki et al., 1991).

2.1. Characteristics for an Ideal Sensor

The performance of a sensor is associated with accuracy of the value according to true value. In order to characterize the validity of analytical results, the following units are prevalently used:

- ✓ Accuracy: Accuracy is the relation between the measurement result and true value. It can be considered as the deviation from the true value. To exemplify, if an oxygen sensor in room conditions measures the oxygen concentration as 21.01% and the true value is 21%, which means this sensor has good accuracy.
- ✓ Precision: It is the degree of the closeness of measurement results to each other. Standard deviation (STD) is the generally accepted way to express precision.

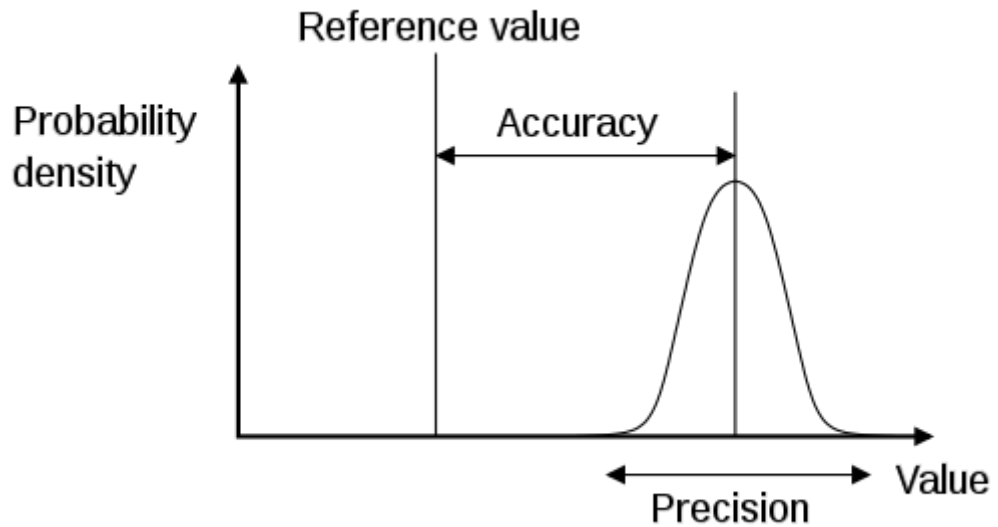


Figure 2.3. Examples of accuracy and precision

- ✓ Resolution: It is the smallest change that a sensor can detect in the quantity to be measured.
- ✓ Sensitivity: Sensitivity of a sensor shows how much the output of the sensor changes when the measured quantity changes. In other words, sensitivity is defined as the ratio between output signal and measured property.
- ✓ Noise: It is defined as random change in measured signal varying in time.
- ✓ Reproducibility: The closeness of agreement among repeated measurements of outputs for the same input where this input is approached from any direction and these measurements are made over a period of time.
- ✓ Linearity: The relation between output signal and gas concentration. Usually the values for linearity are specified for a definite concentration range.
- ✓ Saturation: There are certain limits of detection of each sensor.

Ideally, it is expected that the sensor's output should produce a linear behaviour. However, these values may not show linear response after certain concentrations due to nature of the receptor material. When a sensor, in particular, does not give linear response and shows constant value at high concentrations, that means the sensor reached the saturation value. (Figure 2.4)

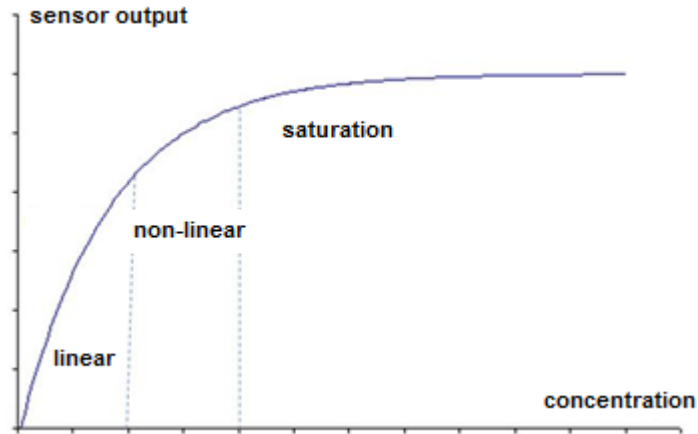


Figure 2.4. Dependence of signal generated by sensor on concentration

- ✓ Interference: If a gas sensor does not always detect the target gas molecules and other gas molecules in the environment affect the measurement results, this situation is called as interference.

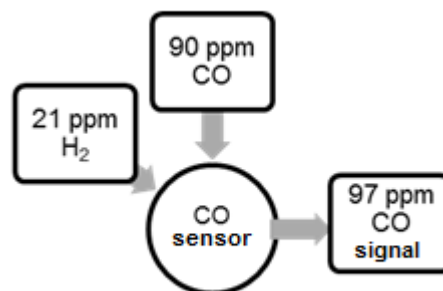


Figure 2.5. Example of interference in gas sensors

- ✓ Reaction time: It is typically the period of time that is needed for a sensor to detect and read a certain gas concentration and the period of time needed for output signal to go to its initial value in a clean environment.
- ✓ Zero and span shift: Zero calibration sets of output of a sensor to zero when the measured property is zero. Span calibration is the maximum output signal of sensor when there is full concentration of target gas. The maximum and minimum limits are determined using these values, the behaviour of sensor

response between these maximum and minimum values determines whether it is linear or should be expressed as mathematical function.

- ✓ Hysteresis: It is the maximum difference in output when the value is approached with an increasing and a decreasing analyte concentration range(Bochenkov and Sergeev, 2010). Infrared sensors usually show no tendency of hysteresis, solid-state sensors like electrochemical and catalytic do, though. It is a very significant parameter for a sensor to give actual value in the calibration phase.

2.2. Types of Gas Sensors

Solid-state gas sensors generate signals depending on change in conductivity, capacitance, work function, mass, optical characteristic or energy in gas/solid reaction as a result of varying concentration of target gas molecules by using organic or inorganic compounds as sensing material. Basically, organic or inorganic (metal oxide semiconductor) materials are coated on the detection surface of a device in the form of thick or thin film in order to create a gas-sensitive active region. The process of reading signals occurs via electrodes, diode, transistor, surface-wave components, the thickness mode transducers or optical apparatus on the device. Despite measuring similar physical parameters, different type sensors have caused different types of technologies. Solid-state gas sensors are basically used for commercial and research purposes in device types as listed in Table 2.2 which is prepared according to the physical changes used in design and gas detection(Capone et al., 2003).

Table 2.2. Types of solid state gas sensors with the corresponding physical change used as gas detection principle

Type of devices	Physical change
Semiconductor gas sensor	Electrical conductivity
Field effect gas sensors: diodes, transistors, capacitors	Work function (electrical polarisation)
Piezoelectric sensors : Quartz crystal microbalances (QMB), surface acoustic wave (SAW), micro cantilevers	Mass
Optical sensors (fibre optic or thin film)	Optical parameters: SPR, reflection, interferometry, absorption, fluorescence, refractive index or optical path length
Catalytic gas sensors: Seebeck effect, pellistors, semistors	Heat or temperature
Electrochemical gas sensors (potentiometric or amperometric)	Electromotive force or electrical current in a solid state electrochemical cell

In this section, information about types of solid-state gas sensors, listed in Table 2.2, will be presented.

2.2.1. Semiconductor Gas Sensors

Semiconductor gas sensors are generally metal oxide based gas sensors. Absorption of gas molecules on the oxide layer result in the catalytic reduction reaction and as a result of this reaction, the electrical resistance of the oxide material changes. The amount of change depend on the speed of the reaction, in other words, it depends on the concentration of gas molecules. Sensor surface needs to access a specific temperature so that the chemical reaction can take place, depending on the material used in the metal oxide. The required temperature is usually between 200 and 250 °C.

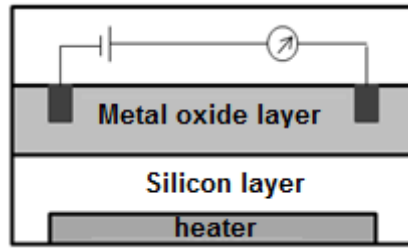


Figure 2.6. Basic components of metal oxide based semiconductor gas sensor

2.2.2. Field Effect Transistor (FET) Gas Sensors

In Field Effect Transistors (FETs), electric field is used to control the shape and hence the conductivity of a channel of one type of charge carrier in a semiconductor material. The FET devices, when used as a converter, convert varying physical and chemical signals into measurable electrical current. Although there are many different FET device developed for different purposes, MOSFET devices are widely used for gas sensor applications.

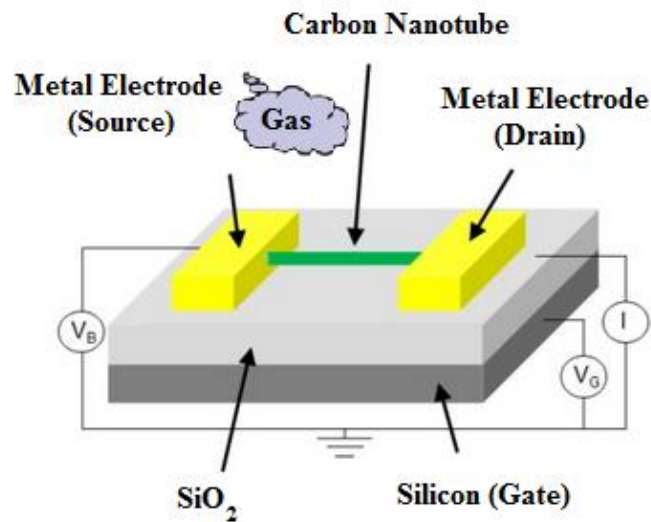


Figure 2.7. Basic structure of FETs

The simplest structure of MOSFET device consists of drain, source and gate which are developed on silicon oxide insulator. The electrical conductivity of the sensor

material placed between source and drain and hence I-V characteristic of transistor depend on the gas concentration of the environment.

2.2.3. Optical Gas Sensors

Optical sensors play an important role in sensitive measurement of chemical and biological quantities. The first optical chemical sensor used a method which measures changes in the absorbance spectrum. Today, a variety of optical methods like ellipsometry, spectroscopy, interferometry, surface plasmon resonance device (SPR) are used for chemical detection and biosensor applications. The values in these sensors are determined by measuring the refractive index, the absorbance and fluorescence properties of analyte molecules. In Figure 2.8, optical components of a system which was used for NO₂ sensing application was displayed (Richardson et al., 2006a).

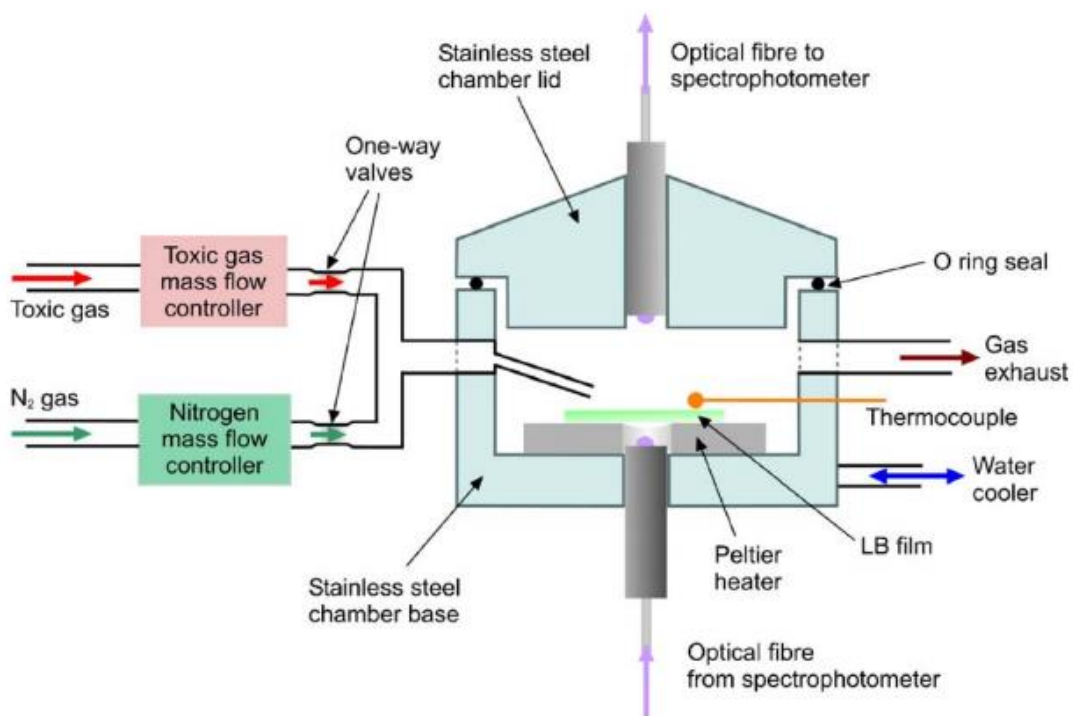


Figure 2.8. Optical apparatus used for NO₂ gas sensing application

2.2.4. Electrochemical Gas Sensors

Electrochemical gas sensors are based on measuring the electrical signal of electrodes which are the results of chemical reaction occurring between the target gas molecules. The gas molecules passing through hydrophobic membrane starts oxidation-reduction mechanism by reacting with the active electrode. The electric signals depending on gas concentration are processed through a circuit connected to the electrodes. There are generally two electrodes in an electrochemical sensor cell one of which is referred to as the active electrode and wherein the chemical reaction takes place. In order to measure electrochemical potential energy of the electrolyte and the electrode, a third electrode can be found as a reference electrode. This reference electrode is used to correct errors caused by the active electrode. The active electrode is made of typically noble metal or materials which are coated with platinum, palladium, carbon. To obtain a measurable signal, electrodes must have a sufficiently large surface area in contact with the analyte. The electrode materials, specifically developed for the gas of interest, catalyses these reactions. A current that is proportional to the gas concentration flows between the anode and the cathode with the help of a resistor connected across the electrodes. In order to determine the gas concentration, the current can be used. Due to the fact that the power consumption of electrochemical sensors is the lowest among all sensor types available for gas monitoring, the sensors are widely used in portable instruments that contain multiple sensors. The cell can measure the electrical signals as current, potential, conductivity or capacitance. In Figure 2.9, schematic representation of a typical electrochemical sensor is given and it includes a sensing electrode and a counter that is used as electrode separated by a thin layer of electrolyte(Chou, 2000).

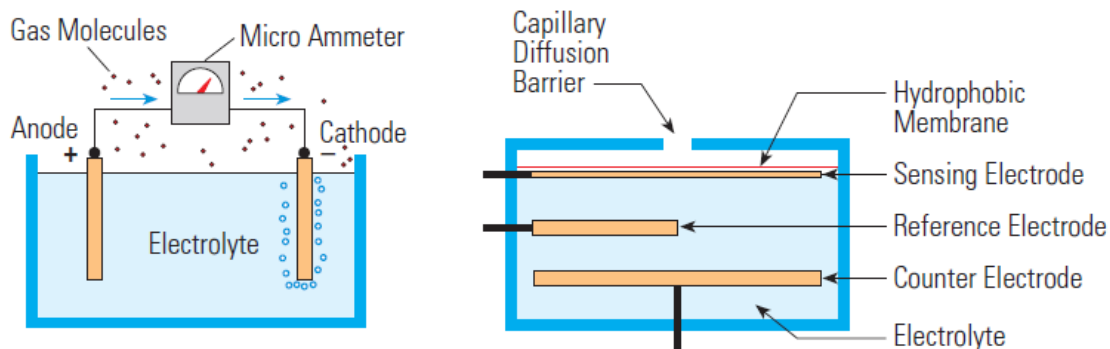


Figure 2.9. Basic electrochemical gas sensor (left) and typical electrochemical gas sensor with three electrodes design (right)

Electrochemical gas sensors are widely used at homes and industries because they are simple, inexpensive and have high sensitivity to gas molecule. They are classified as potentiometric, amperometric and conductivity according to their working principles.

2.2.5. Catalytic Gas Sensors

Called as pellistors, catalytic gas sensors are known as the first chemical gas sensors and they have been in use for more than 50 years to detect the presence of combustible gases. They were also used to monitor gas in coal mines at first. Because of having simple structure, manufacturing of it is easy. In its simplest form, as used in the original design, it was comprised of a single platinum wire. Catalytic bead sensors have been produced in all over the world by a large number of different manufacturers, but the performance and reliability of these sensors varies widely among these various manufacturers. The working principle of a catalytic gas sensor is based on gas oxidation: the combustible gas coming in contact with the catalyst surface is oxidised. The reaction, releasing heat, gives rise to changing of the resistance of the wire. A catalytic gas sensor is a kind of calorimeter and the coils are typically made from platinum wire in order to provide stability with known temperature characteristics. This type of gas sensors is sensitive to hydrocarbon-based flammable gases.

2.2.6. Piezoelectric Gas Sensors

Piezoelectric crystals (quartz crystal microbalance (QCM)) and surface acoustic wave method (SAW) are implemented for sensor applications that use the piezoelectric nature. Discovered first by Lord Rayleigh, SAWs are also known as Rayleigh waves. There are numerous applications areas of surface acoustic wave technology including filters, oscillators, transformers, and sensors. A SAW is a type of mechanical wave motion travelling along the surface a solid material and its amplitude decays exponentially with depth into the substrate. A general property of all types of SAWs is that the energy is mostly localized near the surface, within a depth of about one wavelength. The energy spreads out in the two-dimensional interface region instead of propagating throughout the whole three-dimensional medium, meaning that the propagating wave is confined to the top surface of the substrate(Hess, 2002). On account of this, the SAW is quite sensitive probe to investigate mechanical and electrical properties on the surface of it. A basic structure of a SAW device is illustrated in Figure 2.10.

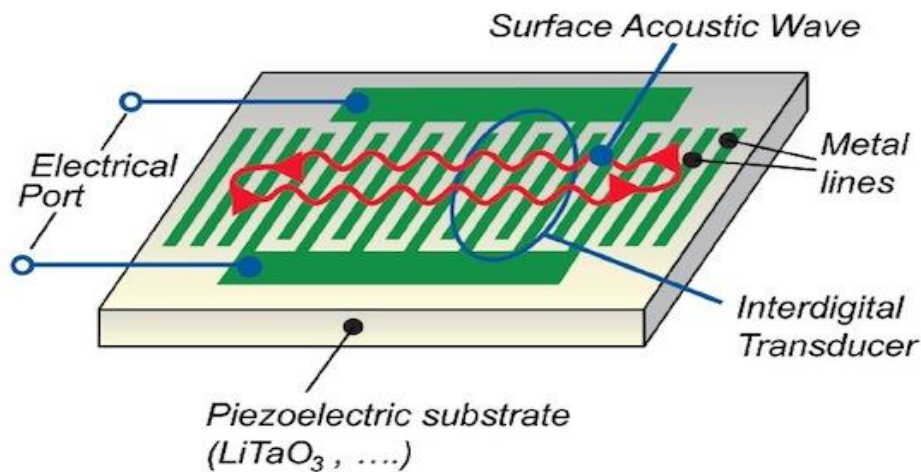


Figure 2.10. Basic structure of a SAW device

Today, SAWs are generally used as chemical gas and biosensor. A basic SAW consists of two interdigital transducers (IDTs) on a piezoelectric substrate such as quartz to convert electrical energy into an acoustic wave. The input IDTs launches SAW whereas the output IDTs receives. Response of gas sensor to the analyte is

determined by calculating phase shifts of progressive acoustic waves moving along the surface of the material. Being one of the piezoelectric based gas sensing method, Quartz crystal microbalance (QCM) technique will be discussed in section 2.3 in detail.

2.3. Theoretical Foundations

2.3.1. Piezoelectric Effect and Principle of QCM

The piezoelectric effect is the property of a material to convert electrical signals into mechanical energy and mechanical energy into electrical signals. Piezo is a Greek word and its means “press”. Piezoelectric effect was first discovered by Pierre and Paul-Jacques Curie in 1880-81. They realized that when an external force was exerted on single crystal of some specific materials, like quartz, they generated a surface charge on the crystals that is proportional to the mechanical pressure applied to the related material. Conversely, after one year, they also discovered applying voltage will give rise to the mechanical deformation of the crystal lattice(Kirschner). Since piezoelectric material converts electrical energy into mechanical energy, it is used in actuator technology. Piezoelectric materials can be classified as ceramic and crystal materials that are non-conductive materials. In addition, this effect is merely seen anisotropic crystalline materials. The polarization of the unit cell (net spontaneous charge distribution) will be zero, if the unit cell of a crystal is isotropic (symmetrical). Unit cells with asymmetric structure (anisotropic) show a net polarity, though(Madou, 2002).

BaTiO₃, PbTiO₃ - PbZrO₃, synthesized from the oxides of lead, titanium and zirconium, are well known piezoceramics. In addition, special doping of leadzirconate-titanate ceramics (PZT) with Ni, Bi, Sb, Nb ions make it possible to adjust individual piezoelectric and dielectric parameters as required. These materials are not ferroelectric above a characteristic temperature, known as the Curie temperature. The Curie temperature (T_c) is used to describe the temperature where a material's spontaneous electrical polarisation changes to induced electric polarisation, or vice versa. It is known that ferroelectric, dielectric (paraelectric) and piezoelectric all have electrical polarisation. There is a spontaneous electrical polarisation when no electric field is present in ferroelectric materials, whereas for dielectric materials there is electrical polarisation aligned only in the presence of an electrical field for them. However,

piezoelectric materials have electrical polarisation on account of deformation of structure from pressure (Guinier and Remi, 1989; Hook and Hall, 2000; Myers, 1997). Hence, the materials mentioned above are in a paraelectric state meaning that no dipole is present above T_c . However, below the Curie point of the material, the cubic, electrically neutral crystalline form gives way to lattice distortions, giving rise to the formation of dipoles and rhombohedral and tetragonal crystallite phases, which are of interest for piezo technology.

The idea to use piezoelectric effect as a mass sensor, which is still the basis for many sensor applications, comes from Sauerbrey. He discovered that resonant frequency shifts is caused by mass changes of the material deposited onto the crystal surface, and he also stated that these frequency shifts are independent of the physical properties of the coated material (Sauerbrey, 1959). His findings indicate that with a simple measurement of frequency shift, mass change on the crystal may be observed without having to know the physical properties of the material. Since quartz crystal microbalance method based on piezoelectric effect is an easy technique to implement, it is used in many sensing applications, as well as in thin-film coating systems and thickness monitors.

A quartz crystal microbalance (QCM) consists of a thin quartz disk sandwiched between two metal excitation electrodes. QCM method is based on the frequency shift caused by adsorption or desorption of molecules by material that is coated on surface of QCM analysis. QCMs gained importance for the purpose of monitoring thickness of the film in vacuum coating systems in 1960s and 70s. In a similar manner, the sensitive receptor on electrodes can be used as gas sensors on the basis of adsorption of molecules in the environment (Buck et al., 2004; Janshoff et al., 2000).

Quartz used in this method is one of the most abundant mineral in nature. Pure form of silicon dioxide crystals (SiO_2) is called as quartz. The density of it is 2.65 g/cm^3 , its melting temperature is $1650 \text{ }^\circ\text{C}$. The crystal structure of silicon dioxide changes when it is heated to $573 \text{ }^\circ\text{C}$. Quartz heated more than this transition temperature is called as the beta-quartz, and quartz at below this temperature is called the alpha-quartz. Since alpha-quartzes are superior in terms of mechanical and piezoelectric properties, they are generally preferred in resonator applications.

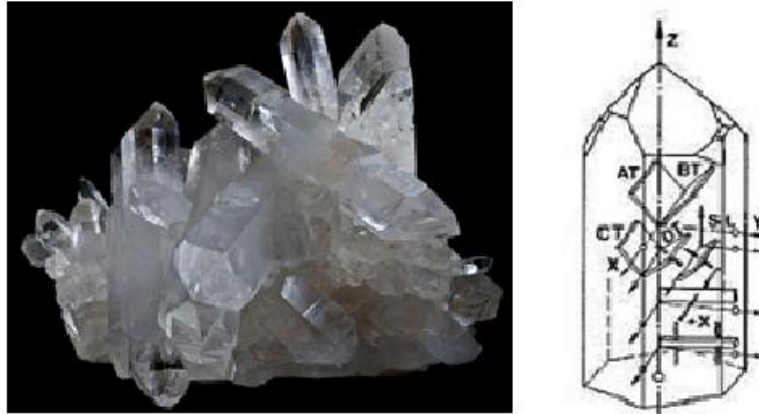


Figure 2.11. Pure Quartz crystal and different quartz crystal cuts

Vibrational frequency of quartz crystal used as resonator depends on the shape or cutting angle of the crystal. Selection of this cutting angle according to the application requirements determines the vibration modes. The AT-cut, BT-cut, SC-cut, IT-cut, FC-cut crystals, which are presented in Figure 2.11, are used for different application purposes. The AT-cut quartz crystal is commonly used in QCM experiments. Only if the quartz crystal plate is cut to a specific orientation with respect to the crystal axes, the acoustic wave can propagate in a direction perpendicular to the crystal surface due to the fact that a QCM is a shear mode device (Ebersole et al., 1990). These specific cuts, shown in Figure 2.12, are representative.

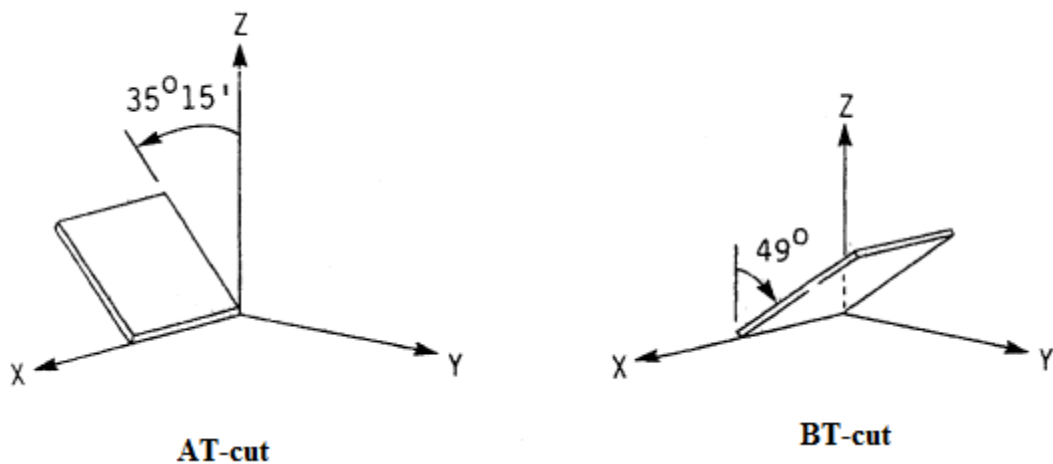


Figure 2.12. AT-cut and BT-cut crystals

Commercially, crystal oscillators having natural frequency of up to 100 MHz can be found. Vibrating crystals in the frequency range of 5-30 MHz are preferred in gas sensor applications. The AT-cut is widely used in QCM applications because of its low temperature coefficient at room temperature, meaning that small changes in temperature only result in small changes in frequency. In Figure 2.13, resonant frequency versus temperature for different cut angles of pure quartzes is given. AT-cut has quite good performance over a wide temperature range. The cut is made from a Y bar at $35^{\circ}15'$ theta rotation because the temperature stemming from heat that is produced by electronic devices is between 50-70 °C. Between this temperature range, the AT-cut quartz crystal (cutting angle $35^{\circ}15'$) has the lowest temperature coefficient.

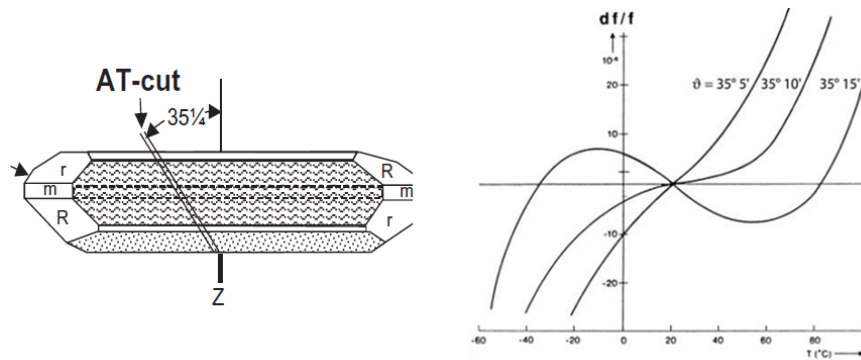


Figure 2.13. AT-cut angle of quartz crystal and natural vibration frequency, temperature and cut angle dependence of quartz crystal

Due to these properties, AT- cut quartz crystals are the most suitable one for QCM applications (Bottom, 1982). In QCM technique, mostly disk shaped oscillators that have basic vibration frequency ranging from 5 to 30 MHz are used. This vibration frequency (f_R) depends on the thickness of crystal, as well. In Figure 2.14, cross-sectional and surface-view of a quartz crystal is seen.

Gold electrodes, which do not interact with the coated material and oxygen, is formed by lithographic techniques or vacuum deposition on both sides of the quartz crystal that is cut in a certain angle and size. The electrodes are used to stimulate the acoustic waves. As seen in figure, receptor chemical material to interact with the analyte gas is coated as a thin film via one of coating methods on these gold electrodes.

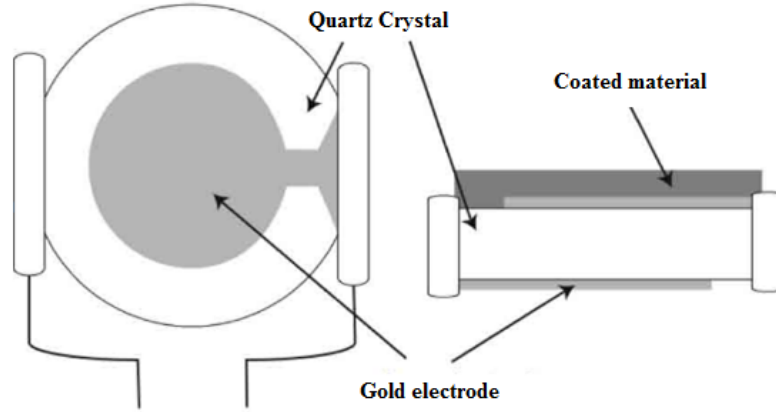


Figure 2.14. Cross-sectional and surface-view of a quartz crystal microbalance

In Figure 2.14, a schematic representation of the quartz crystal of thickness t and weight m are given. At resonance frequency, the wavelength λ is

$$\lambda = \frac{2t}{n} \quad (2.1)$$

where n is the harmonic number. This equation holds true since the QCM is piezoelectric material and an oscillating electric field applied across the device induces an acoustic wave propagating through the crystal and meets the minimum impedance (corresponding resonance frequency) *when the thickness of the device is a multiple of a half wavelength of the acoustic wave* (Ebersole et al., 1990). In addition, for $n=1$, the frequency is F and for higher harmonics n should be more than 1. The acoustic shear wave velocity v is defined as

$$v = \lambda F \quad (2.2)$$

therefore, the frequency will be as follows

$$F = \frac{v}{2t} \quad (2.3)$$

The shift stemming from the small change in thickness can be obtained by differentiating both side of last equation with respect to t . After differentiating it, the following equation is obtained;

$$dF = -\frac{v}{2t^2} dt \quad (2.4)$$

Dividing equation 2.4 by 2.3 gives the frequency stability, that is;

$$\frac{dF}{F} = -\frac{dt}{t} \quad (2.5)$$

Equation 2.5 can be written in terms of mass of the coated film per unit area M and change in the mass per unit area ΔM , namely;

$$\frac{\Delta F}{F} = -\frac{\Delta M}{M} \quad (2.6)$$

In this derivation, the net change in mass ΔM is assumed to be homogenously distributed over the surface of the crystal. Therefore, mass change in mass per unit area ΔM is proportional to total mass change on the surface of crystal $\Delta M_{kristal}$. This means acoustic shear wave velocity acts the same over the entire crystal surface. If M and ΔM in equation 2.6 are written in terms of the density of material deposited on unit area of thin film ρ_f and thickness of it t_f , then the frequency stability or relative frequency change will be;

$$\frac{\Delta F}{F} = -\frac{\rho_f t_f}{\rho t} \quad (2.7)$$

In addition, the resonance frequency F in equation 2.3 is substituted in 2.7, then

$$\frac{\Delta F}{F} = -\frac{\rho_f t_f 2F}{v\rho} \quad (2.8)$$

or

$$t_f = -\frac{\Delta F}{2F^2} \frac{v\rho}{\rho_f} \quad (2.9)$$

Here, F , ρ and v are constants that are directly related to the production of crystal. According to this equation, QCM can be used as a thickness monitor if the density of the coated material is known. By using equation 2.8, a crystal constant can be defined, that is;

$$C_q = \frac{2}{v\rho} \quad (2.10)$$

In that case, the relationship between frequency shift and mass change will be;

$$\Delta F = -C_q F^2 \Delta M_f \quad (2.11)$$

Therefore, the change in resonance frequency will be;

$$\frac{\Delta F_p}{F} = -C_q F \Delta M_f \quad (2.12)$$

This equation is known as Sauerbrey equation (Sauerbrey, 1959). Different derivation methods and forms of this equation are also available, however, in essence, the change in mass of the material deposited on the crystal can simply be obtained only with the help of measured resonance frequency shift. That is, the shift in frequency is directly related with the change in mass.

$$\Delta f = -\frac{2f_0^2}{A\sqrt{\mu\rho}} \quad (2.13)$$

In equation 2.13, f_0 , A , μ and ρ are the resonance frequency of fundamental mode of the QCM crystal, the area of the gold disk coated onto the quartz crystal, shear modulus of quartz and density of the crystal, respectively. The QCM, used in this study, works with oscillation frequencies between 7.995 MHz and 7.950 MHz. AT-cut quartz crystals with a fundamental frequency of 7.995 MHz were obtained from International Crystal Manufacturing Co. (ICM). The density (ρ) of the crystal is 2.684 g/cm³, and the shear modulus (μ) of quartz is 2.947×10^{11} g/cm s². That is, around oscillation

frequency of 7.995 MHz, a net change of 1 Hz corresponds to 1.34 ng of gas molecules adsorbed or desorbed onto the crystal surface of an area (A) of 0.196 cm^2 . Sauerbrey equation has been developed to investigate the vibration characteristics of solid materials coated on the electrode in air.

QCM was used only for gas phase applications until 1980. In 1985, QCM measurements were performed in the liquid phase and it was demonstrated that QCM could oscillate in a stable manner in liquid environment (Kanazawa and Gordon, 1985). It was seen that the change in resonant frequency is proportional to the multiple of density and viscosity of liquid.

2.4. Calixarenes

In studies conducted within the area of supramolecular chemistry, new synthetic methods in research topics such as allosteric effect, signal transfer, catalysis, and guest-host chemistry have been developed. In this field, various methods have been applied to synthesize macromolecules having appropriate functional groups. Examples to these materials are crown ethers, kryptans, cyclofans, and cyclodextrines (Bender and Komiyama, 1978; Izatt et al., 1992; Lehn, 1988; Pedersen, 1967; Szejtli, 1988).

Calix[n]arenes are ring-structured macrocyclic compounds, formed by connection of aromatic units via methylene bridges. Known as third generation supramolecular compounds alongside crown ethers and cyclodextrines, calixarenes are obtained by the condensation reaction of phenyl and formaldehyde in basic environments. Etymologically, the word calix[n]arene is from the Greek word “calix” or “chalice”, meaning “bowl” and “arene”, the name of aromatic hydrocarbon structures in chemical nomenclature. The number “n” in square brackets indicates number of rings in the calixarene molecule. Figure 2.15 shows the general structure of calix[4]arene for $n=4$.

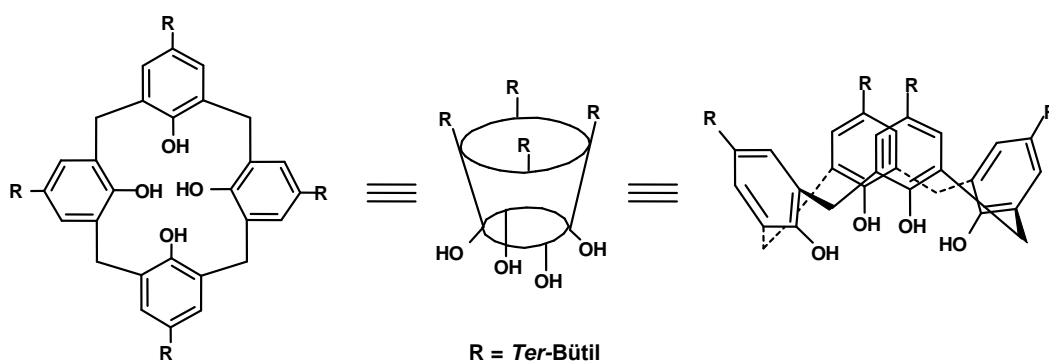


Figure 2.15. General structure of calix[4]arene

German organic chemist Adolph von Baeyer first obtained phenol formaldehyde resin in 1872 by reacting phenol and formaldehyde (von Baeyer, 1872). In the following years, Leo Hendrik Baekeland invented bakelite, which does not dissolve in any organic solvent, insulating and nonflammable, by cross linking the phenol formaldehyde resin which Baeyer had obtained, and patented it in 1908 (Baekeland, 1909). This obtained resin was first known as “phenoplast” and besides being an instant commercial success, it raised the attention of industrial and academic researchers on phenol formaldehyde chemistry. Along these researchers Alois Zinke obtained a product with low solubility and high molecular weight during their studies on macro cyclic compounds by reacting *p*-*ter*-butyl phenol and aqueous formaldehyde in a basic environment, and speculated that this product was a cyclic tetramer (Zinke and Ziegler, 1944). Subsequent developments in the field of macro cyclic compounds revealed that the compound which Zinke had synthesized was not only in a single tetrameric structure but rather was a product mixture (Gutsche and Muthukrishnan, 1978).

Gutsche managed to efficiently synthesize *p*-*ter*-butylcalix[4]arene, *p*-*ter*-butylcalix[6]arene and *p*-*ter*-butylcalix[8]arene separately and with high purity by optimizing the reaction conditions of *p*-*ter*-butyl phenol and formaldehyde in a basic medium (Gutsche and Iqbal, 1990). Today, various (9-20) aromatic ring constituent calixarenes have been synthesized.

NMR studies has shown that calix[4]arene exists in solution with four different conformations: cone, partial cone, 1,3-alternate and 1,2-alternate structures.

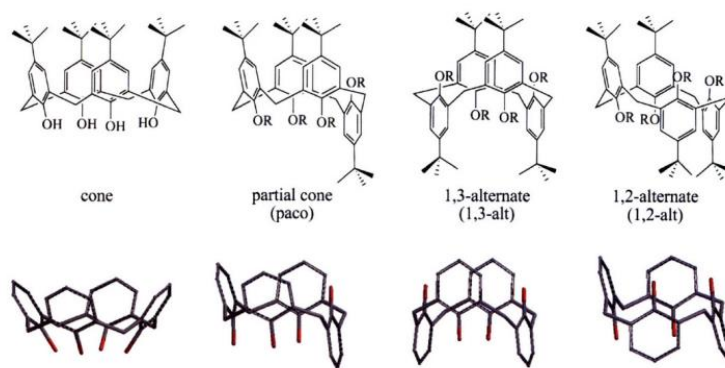


Figure 2.16. Different conformations of p-tert-butyl calixarene

Due to their excellent sorption capabilities and stable structures, calixarenes are valuable compounds for sensor applications.

The primary reason that calixarenes are preferred in favor of other supramolecules in synthesis is their ability to be extensively functionalized either via the p-site of the phenyl ring (upper rim) or the phenolic oxygen (lower rim) by various functional groups depending on the desired purpose (Sayin et al., 2011). Alongside this aspect, both the effect of bonding functional group and calixarenes' ability to make guest-host type complexes drive the utilization of these compounds in many areas, especially sensors.

Hole diameters of phenolic O sites for calix[4]arene, calix[6]arene and calix[8]arene are 3 Å, 7.6 Å and 11.7 Å, respectively. In case designed with appropriate functional groups, calixarenes can selectively carry desired molecules. In this regard, calixarenes can be developed by functionalizing with functional groups such as amine (Ferguson et al., 1987), ester (Zheng et al., 2004), amide (Anthony & McKervey, 1992), ether (Zheng and Zhang, 2004), alcohol (Chang et al., 1987), carboxylic acid (Bocchi et al., 1982) and crown ethers (Arnaudne et al., 1989).

With their excellent sorption capabilities, ability to retain stable structures and technologically viable properties, calixarene compounds used in this thesis are suitable for sensor applications. A variety of studies exist in literature about synthesis of calixarenes with various functional groups, but recently, application related research has increased by the growing interest stemming from utilization of calixarenes as gas and ion sensors based on their guest-host chemistry. In sensor applications; ISFET, ISE, optical transducer and QCM methods are widely used.

Calixarenes, along with crown ethers and cyclodextrines, belong to the supramolecular host group. Supramolecular chemistry investigates intermolecular forces known as “weak forces” such as hydrogen bonding, ion-dipole, dipole-dipole interactions and Van der Waals forces. With respect to the sizes of interacting molecules, supramolecular chemistry is classified as guest-host chemistry, molecular topology and molecular combination.

In order to utilize as chemical sensors, calixarenes must exhibit selectivity and sensitivity to only a defined type of molecule. This peculiarity can be realized by molecular identification principles and guest-host interactions. Host molecules designed with these considerations in mind must bear the features below:

1. Host molecules must be functionalized with structures of chemistry that will bond to detected species with weak electrostatic forces.
2. Host molecule must have adequate molecular space compatible with the detected molecule or ion.
3. Guest or host molecules must yield measurable physical or chemical quantities as they are bonded.

In simplest terms, guest-host chemistry can be explained by the settling of organic guest molecule or ion into the cavity of the bigger macrocyclic host molecule with non-covalent weak bonds. This mechanism is illustrated schematically in Figure 2.17.

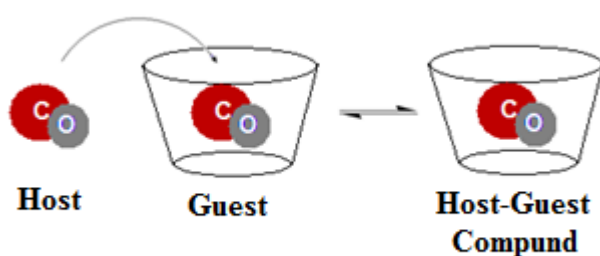


Figure 2.17. Host-guest interactions in supramolecular systems

With their applicability as host molecules, calixarenes are frequently utilized in sensor applications.

In a study, calixarenes, whose chemical structure is depicted in Figure 2.18, were used by alkylation in various conformations as NO₂ sensors (Ohira et al., 2009).

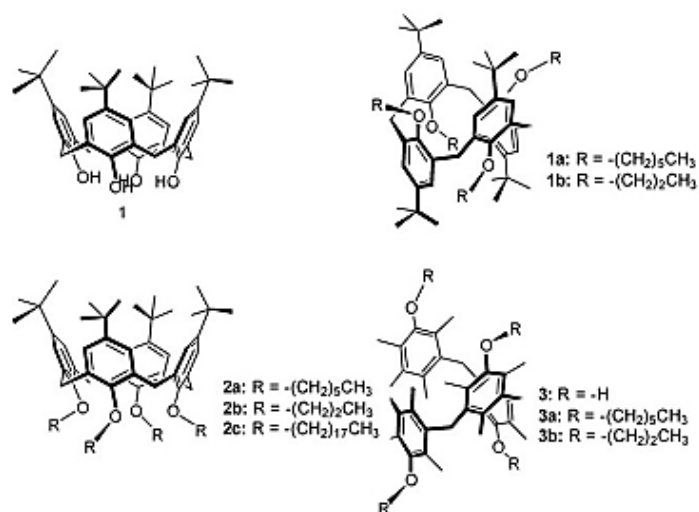


Figure 2.18. Calixarenes used as NO₂ sensor

In another study, acoustic wave sensors which were coated with 4 calixarene compounds that had chemical structures depicted in Figure 2.19 were investigated with piezoelectric transducers. Characteristic frequency responses for 22 volatile organic gases were given. This mechanism was proposed to be formed by the C-H..... π interaction between the methyl groups of volatile organic gases and phenyl ring of the calixarene molecule.

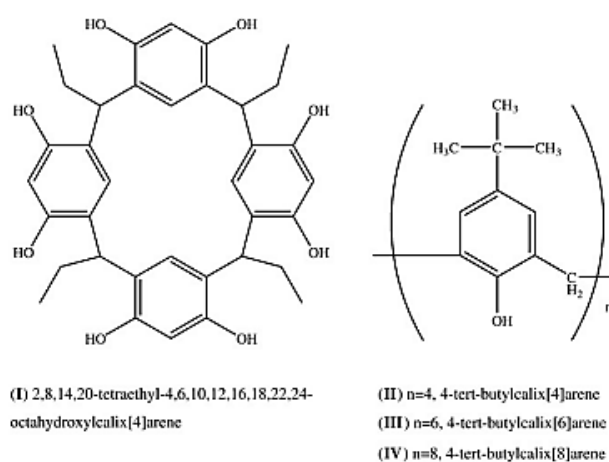


Figure 2.19. Acoustic wave sensor based on calixarenes

In a different study, after functionalizing p-ter-butylcalix[4]arene and p-ter-butylcalix[6]arene molecules with different groups, design and production of chemical gas sensor series depending on discontinuous gold films' conductive modulations deposited over dielectric substrates were investigated (Filenko et al., 2005; Kalchenko et al., 2002). Reactions of these calixarene structures to alcohol derivatives such as H₂O, MeOH, and EtOH were electrically measured.

In another work, sensitivity studies were conducted against NO₂ gas concentrations varying between 0.13 and 4.6 ppm by forming Langmuir-Blodgett (LB) films with calix[8]arene molecules functionalized with C(CH₃)₃ and CH₂CO₂ groups and sensitivity of synthesized calixarenes under 1 ppm NO₂ gas concentration was reported (Richardson et al., 2006b).

In a study which QCM method was involved, calixarene molecules, whose structures were depicted in Fig. 2.37, were covalently bonded onto gold QCM electrodes by SAM (self-assembled monolayer) technique and their sensitivity characteristics to various butylamine volatile gases were investigated (Yuan-Yuan et al., 2005).

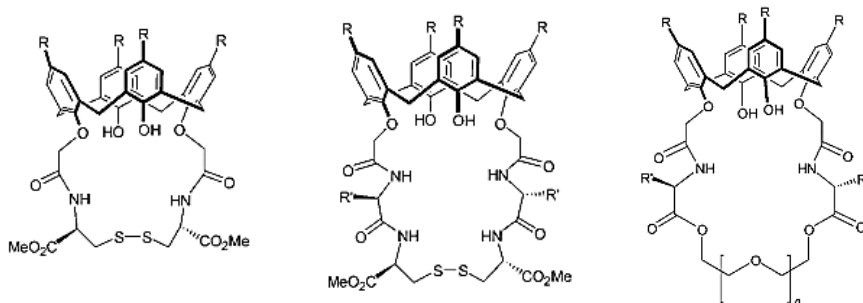


Figure 2.20. Calixarene molecules synthesized to detect volatile organic compounds

In other studies calixarene molecules were employed as sensor materials, quartz crystal sensor arrays were formed with calix[4, 6, 8]arene molecules bearing different functional groups by using vacuum thermal coating, thin/thick distillation, LB, and spray techniques and selectivity-sensitivity characteristics of these arrays to volatile organic compounds such as benzene, toluene, chloroform, dichloromethane, chlorobenzene were assessed in three different gas systems via QCM

technique(Kalchenko et al., 2002; Koshets et al., 2005). Humidity sensor studies conducted with calixarene molecules also exist in literature. Using p-sulphonatecalixarene derivatives, Okur et al. investigated their responses under varying environmental humidity conditions by QCM method(Okur et al., 2010).

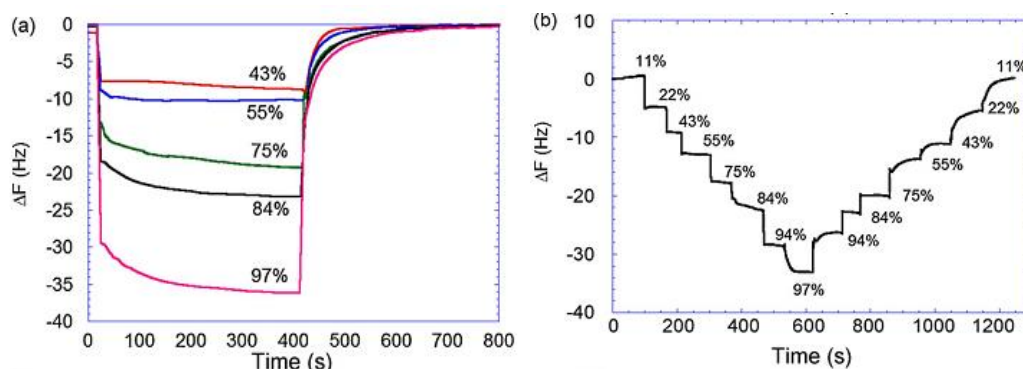


Figure 2.21. Humidity sensing properties of a sulphonate calixarene derivative

In recent literature, sensor studies were conducted with calixarenes using converters such as ISFET and ISE to detect some metal anion and cations. Some of these studies can be referred as follows; Ag^+ (Chen et al., 2000), Hg^{2+} (Talanova et al., 1999), Ni^{2+} (Ma et al., 2001), Th^{4+} (Demirel et al., 2003), Na^+ (Kimura et al., 1990), K^+ (Katsu et al., 2005), Cd^{2+} (Zhang and Huang, 2001), Pb^{2+} (Buie et al., 2008), Mn^{2+} (MALKHEDE et al., 1999), Co^{2+} (Gupta and Khopkar, 1995) and Tl^+ (Talanova et al., 2005).

In current literature, materials such as SnO_2 , ZnO , ZnO-CuO , In_2O_3 , $\text{WO}_3\text{-In}_2\text{O}_3$ have been studied by various different methods to detect the carbon monoxide (Choi and Choi, 2000; Khatko et al., 2005; Yoon and Choi, 1997). However, no study has investigated carbon monoxide sensing applications with iron doped calixarene molecules.

CHAPTER 3

EXPERIMENTAL DETAILS

In this study, the sensitivities of various iron doped and undoped calixarene molecules to CO gas were investigated by using QCM technique and measuring the change in electrical resistance. In this section, the gas flow system and measurement system designed to carry out this study, the photolithography technique used to fabricate interdigitated electrodes (IDE) and sensor design, iron doping process of functional calixarene molecules and preparation of thin films of these molecules are described in detail.

3.1. Gas Flow Control and Measurement System

The designed system consists of three main parts. The first part sends the adsorption and desorption gas to the test cell by using the gas flow meters connected to the gas control unit. In the second part, there is a leakproof gas test cell. The undoped and doped calixarene films coated on QCM and IDE electrodes gave response as a signal to the sent gas. While the signals coming from QCM with a frequency counter connected to a computer, the electrical signals are measured with a computer-controlled Keithley 2636A with constant DC voltage between gold electrodes.

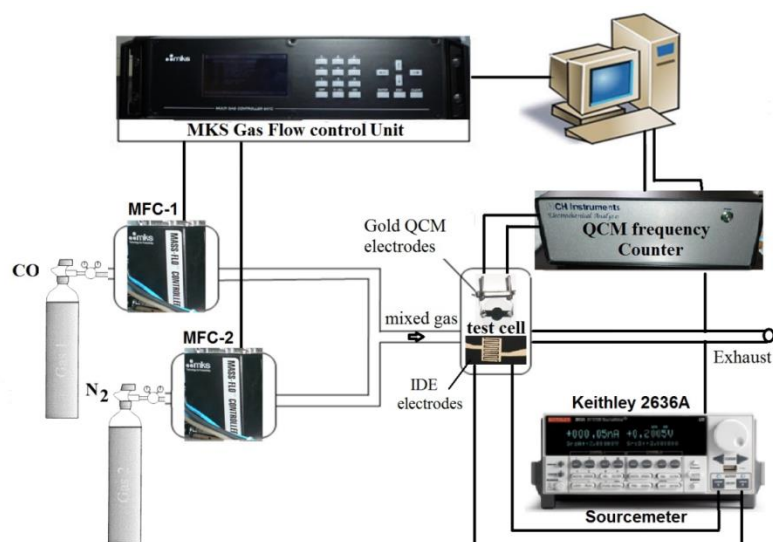


Figure 3.1. Schematic of gas flow system

A schematic of the experimental setup is shown in Figure 3.1. A time-resolved electrochemical quartz crystal microbalance (EQCM) with the model of CHI400B Series from CH Instruments (Austin, USA), shown in Figure 3.2, was used to measure the change in the resonance frequency of quartz crystals between gold electrodes via both serial and USB interface connected to a computer. The QCM works with oscillation frequencies between 7.995 MHz and 7.950 MHz. AT- cut quartz crystals with a fundamental frequency of 7.995 MHz were obtained from International Crystal Manufacturing Co. (ICM). The density (ρ) of the crystal is 2.684 g/cm^3 , and the shear modulus (μ) of quartz is $2.947 \times 10^{11} \text{ g/cm s}^2$. According to the Sauerbrey equation, around oscillation frequency of 7.995 MHz, a net change of 1 Hz corresponds to 1.34 ng of gas molecules adsorbed or desorbed onto the crystal surface of an area of 0.196 cm^2 . Gas flow into test cell are supplied by two CO and N_2 calibrated mass flow meters (MKS,179A Mass-Flo®) and RS232 controlled gas flow control unit (MKS).



Figure 3.2. CHI400A EQCM



Figure 3.3. Coated and uncoated QCM electrodes

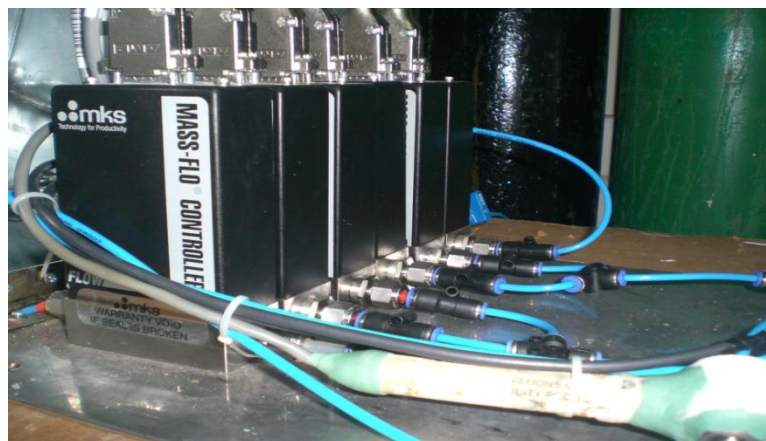


Figure 3.4. MKS 179A Mass-Flo® flow meters

A multichannel controller providing both pressure and flow control with the model of 647C Four channel Mass Flow from MKS Instruments has been used to control the mass flow meters. MKS instrument is controlled via RS232 interface using labview program. With the gas flow rate, the desired interaction times can be controlled. MKS 647C and Keithley 2636A are displayed in Figure 3.5.



Figure 3.5. MKS 647C and Keithley 2636A Sourcemeter

In this study, high purity nitrogen (N_2) gas is used as desorption gas, while the tested CO gas with a concentration of 10000 ppm is used as active gas. The adsorption and desorption kinetics of coated films can be investigated by both QCM and IDE

electrodes fabricated by using lithography techniques, hence these are the methods used to study sorption kinetics of iron doped and undoped various calixarene molecules. The gas test cell is put in a metal box so that it is not affected by environmental effects and this box is always pumped down in case of gas leakage. In addition, an industrial CO gas detector from Industrial Scientific with the model of M40, sensitive to even 1 ppm of CO, was used for gas leakage security purpose. The entire system was also remote controlled to carry out studies safely. In Figure 3.6, the experimental system, including gas test cell, is illustrated.



Figure 3.6. The box including test cell and the whole experimental setup

3.2. Device Fabrication (IDE): Photolithography Technique

In order to fabricate interdigitated electrodes, photolithography technique was utilized. Fabrication of IDE requires well cleaned substrate. Hence, the process was started with cleaning procedure. Ultrasonic cleaning was used for cleaning process to remove some defects stemming from dust or some other types of particles. Glass used as substrate was rinsed in acetone, ethanol, iso-propyl alcohol and water for fifteen minutes in ultrasonic cleaner, respectively. Then, nitrogen was used to dry substrate. Finally, plasma cleaning (with oxygen plasma) process was performed. Plasma cleaning with oxygen plasma removes neutral and technical oils and grease at nanoscale and reduces contamination as seen in Figure 3.7.

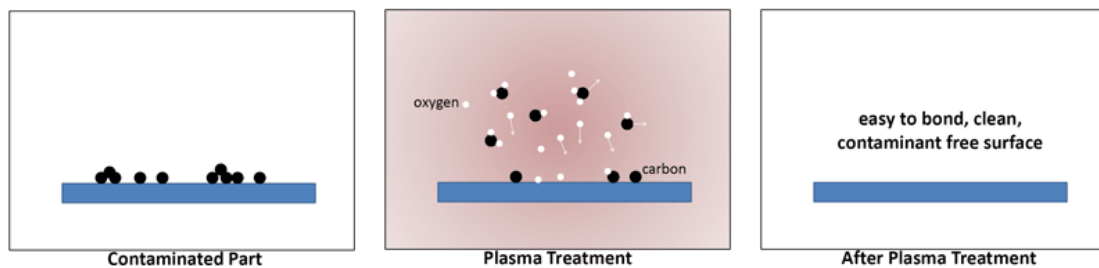


Figure 3.7. Schematic of plasma cleaning procedure

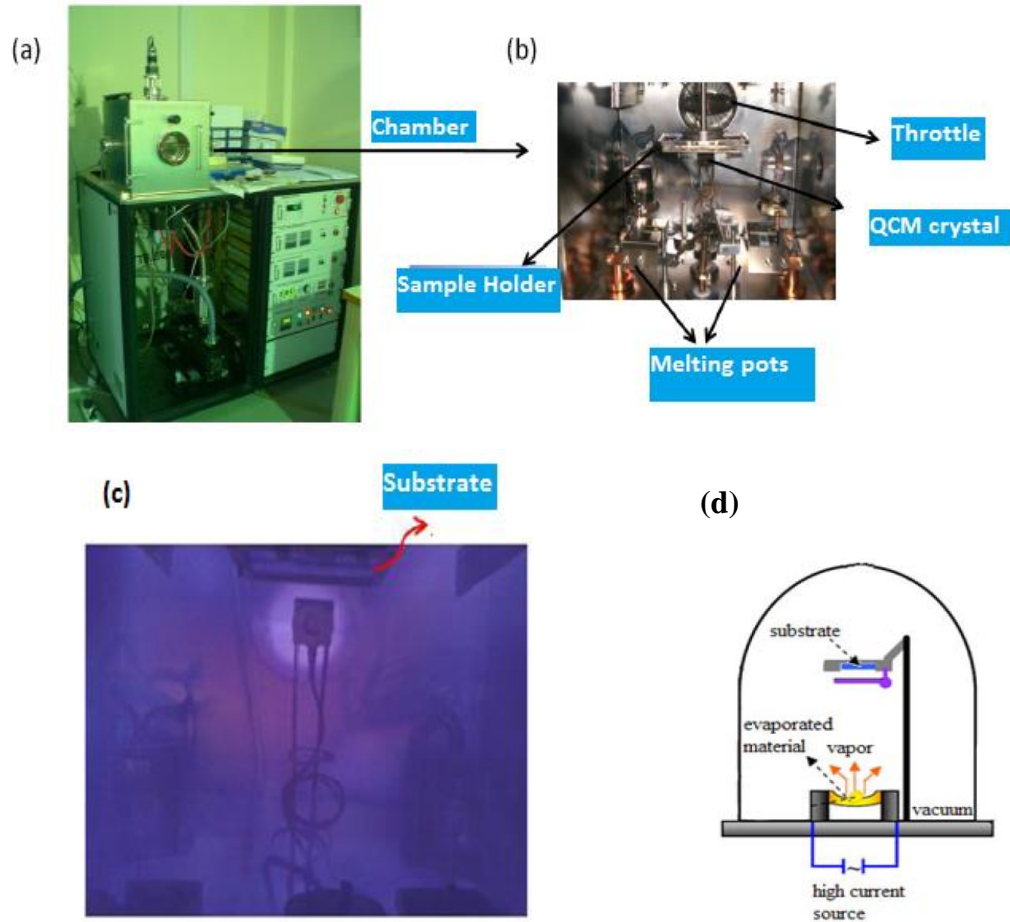


Figure 3.8. (a) and (b) Evaporation system with plasma cleaning option (c) during plasma cleaning (d) schematic of evaporation

Figure 3.8 illustrates the evaporator system, equipped with plasma cleaning system. In this system, energetic oxygens are used to remove contaminants. This cleaning procedure made substrate suitable for lithography process.

After the cleaning procedure, the vacuum thermal evaporation technique seen in Figure 3.8(d) was used to deposit metal layers on substrates. This technique includes evaporation of the material in filament boat heated by high current source and recondensation of the material with vapour state onto cooler substrate. Deposition and thickness of film on the substrate are controlled by a shutter and it also provides good quality thin films which does not have contamination coming from other materials in the boat at the starting of evaporation. For the good quality thin film, evaporation was done in vacuum around 10^{-6} Torr. First the glass substrates were coated with a few nanometer chromium layer. The Cr was used as interlayer between gold and substrate

since Cr gives good mechanical adhesion. Then, a gold layer with a thickness of 60 nm was deposited on Cr layer by using thermal evaporator.

After coating substrate with Cr and gold, respectively, the process continued with the photolithography procedure including following steps; spin coating, soft (pre) baking, alignment and exposure, developing and etching. The photolithography steps were performed in class 1000 clean room as illustrated in Figure 3.9.



Figure 3.9. Class 1000 clean room

There are two types of photoresist which are used in micro fabrication; positive and negative photoresist. Both of the resists consist of organic molecules. When a positive resist is exposed to UV, the polymers break up in smaller parts. Breaking of chains makes the exposed material more easily dissolvable. When the resist-coated substrate immersed into a special solvent, only the resist in exposed parts will be washed away. The process will be reversed for the negative photoresist. That is, when a negative photoresist is exposed, the monomers will cross link and forms polymer which is no longer dissolvable. Only the photo resist in exposed areas will remain on the surface after the development. In spin coating step, spin coat Ge-8 (from Speciality Coating System, Inc.) was used as a spin coater as depicted in Figure 3.11. AZ 1505 was used as positive photoresist. Spin coating process was performed at 4600 rpm for 50 s.



Figure 3.10. Photolithography steps. (1) cleaning, (2) Cr film deposition, (3) Au film deposition, (4) positive resist coating, (5) UV light exposure, (6) development, (7) Au etching, (8) Cr etching

After spin coating, soft baking was applied in order to improve photoresist-sample surface adhesion and promote uniformity and drive off most of solvent in photoresist. In our experiments, baking temperature and time were respectively determined as 90°C and 50s on a hot plate (see Figure 3.11) by taking photoresist characteristics into account.

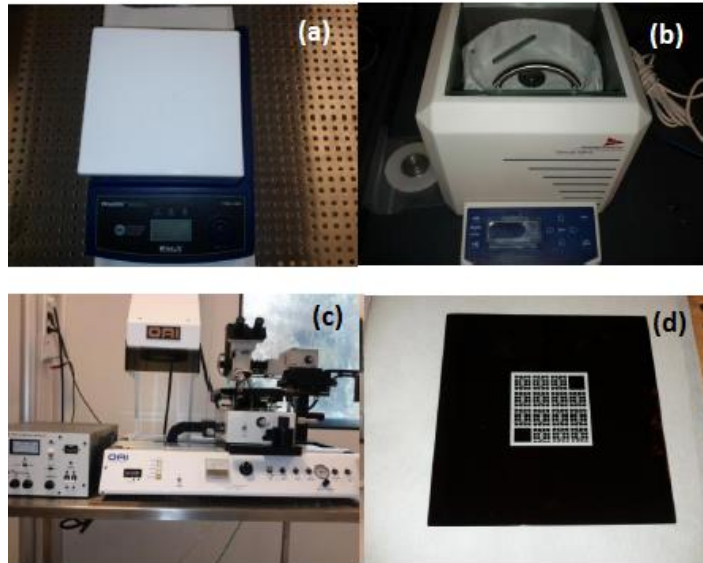


Figure 3.11. (a) Hot plate, (b) spin coater, (c) mask aligner and (d) mask

Transfer of mask image, illustrated in Figure 3.12, to the resist coated sample occurred in alignment and exposure step by activating photosensitive components of photoresist. (The width and separation of fingers are $3\mu\text{m}$.) Hence, in this step, a mask aligner system from OAI was used, as seen in Figure 3.11. After several training, the appropriate exposure time was determined as 3s for our work. After exposure of photoresist, the sample was dipped into the developer (AZ 726 MIF) for 3s to remove the exposed area. Then, the sample was dipped into distilled water to stop the developing process. At the end of the step, visible patterns appeared on the sample and the sample was inspected to verify the quality of pattern via optical microscope.

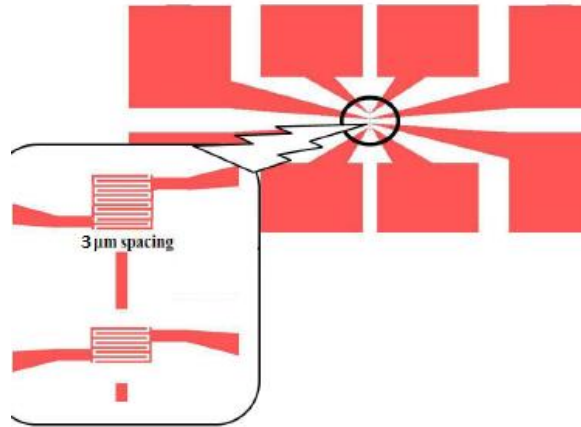


Figure 3.12. Mask design used to expose positive photoresist

The photolithography process has determined up to now. After lithography, there would be regions without resist on the surface of sample. That is, the unexposed areas remained as protective layer. The next step was to remove Au layer on which there was no photoresist. Hence, a chemical solution called Aqua regia (nitrohydrochloric acid) which is a highly corrosive mixture of acids formed by freshly concentrated nitric acid and hydrochloric acid in a volume ratio of 1:3 was used to remove Au gold layer, as seen in Figure 3.13(a). This solution etches or dissolves gold layer. After dipping sample into aqua regia for approximately 5s, the sample was put into distilled water to stop etching process. The step after etching gold layer is to remove Cr layer. In order to get rid of Cr layer, Cr etchant which was bought from microchemicals was used. (see Figure 3.13(b))

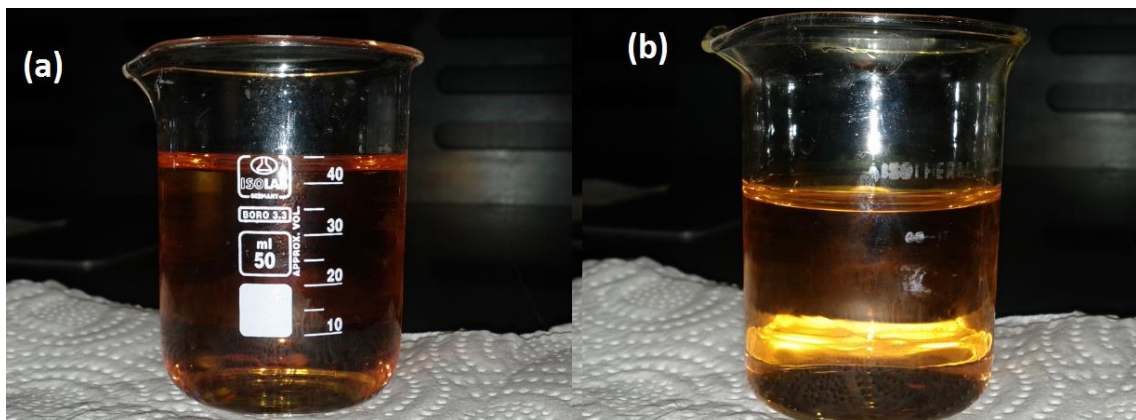


Figure 3.13. Aqua regia (Au etchant), (b) Cr etchant

After removing Cr layer, the photoresist used as protective layer was removed by dipping sample into acetone in ultrasonic bath for 10 minutes. In order to clean sample, it was dipped in isopropanol in ultrasonic cleaner and finally nitrogen was used to dry the sample.

At the end of processes, desired pattern was created on substrate. Table 3.1 summarizes all parameters used in photolithography process.

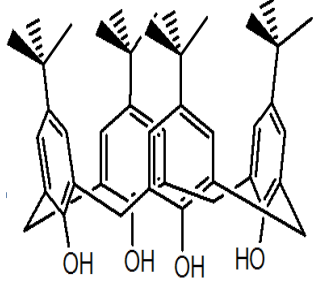
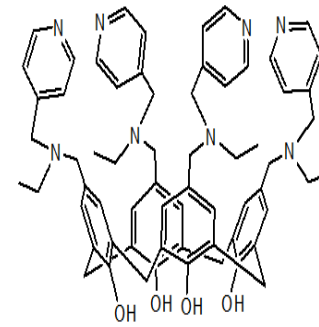
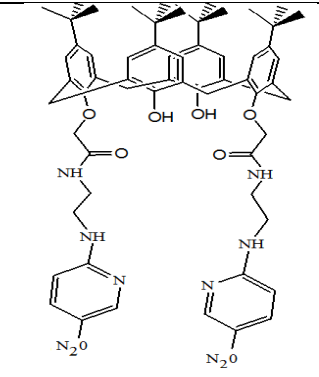
Table 3.1. The parameter values used in photolithography process

Photoresist	Spin speed	Softbake and temperature	Exposure time	Development time
Positive	4600 rpm	50 sec, 90 ⁰ C	~3 sec	~3 sec

3.3. Iron Doping Procedure of Various Functional Calixarene Molecules and Preparation of QCM Electrodes

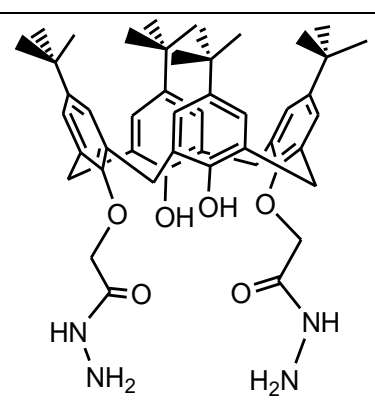
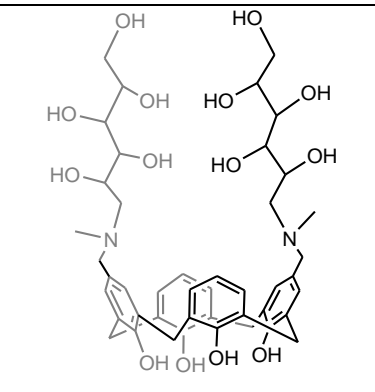
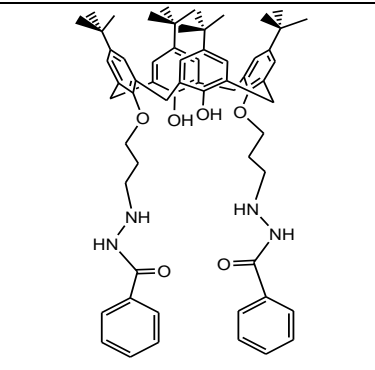
When doping calixarene molecules with iron, the calixarene molecules, which contain amine groups, were preferred so that the acid-base reaction could take place. The molecular structure and chemical name of calixarene molecules used in this thesis are given in Table 3.2. The calixarene molecules used in this thesis have been synthesised by Prof. Dr Mustafa Yılmaz, Serkan Sayın and his group in Selçuk University. The synthesis procedures of two calixarene molecules are briefly given. Since this thesis is supported by Turkish Scientific Association (TUBITAK) under project number TBAG 109T240, the information about synthesis process of other calixarene molecules can be found in final report of that project.

Table 3.2. Molecular structures and chemical names of each calixarene molecule used in this thesis

Molecules	Chemical name	Molecular Structure
Calix 1	p-tert-butyl calix[4]arene	
Calix 6	5,11,17,23-tetra-4-(ethyl amino methyl) pyridine-25,26,27,28-tetra-hydroxy calix[4]arene	
Calix 8	2-(2-Aminoethyl Amino)-5-nitro pyridyl containing calix[4]arene diamide derivative	

(cont. on next page)

Table 3.3 (cont.)

Calix 17	5,11,17,23-tetra-tert-butyl-25,27-di hydrazine amide carbonyl metoxy-26,28-dihydroxy-calix[4]arene	
Calix 18	5,17-bis[(N-methylglucamine)methyl]-25,26,27,28-tetrahydroxycalix[4]arene	
Calix 19	5,11,17,23-tetra-tert-butyl-25,27-di(benzhydrazidylmetoxy)-26,28-dihydroxy-calix[4]arene	

The synthesis process of calix 18 and calix 19 are given below.

Synthesis of Calix 18 (5,17-bis[(N-methylglucamine)methyl]-25,26,27,28-tetrahydroxycalix[4]arene):(Sayin et al., 2010)

4 mL of glacial acetic acid, 26.085 mmol of N-methylglucamine, and 37% aqueous formaldehyde (1.25 mL) were added into a solution of 4.7 mmol of calix[4]arene, synthesized according to previous procedure (Gutsche and Nam, 1988), in 150 mL of THF. The resulting solution was stirred at room temperature for 20 days

while monitored by TLC. Before adding methanol, the solvent has been removed under vacuum. The remaining precipitate was filtered off and was evaporated. The received product was washed with water and dried under vacuum. 39% yield: mp: >350°C ¹HNMR (400 MHz DMSO): δ 2.49 (s, 6H, -CH₃), 3.16–3.63 (br, 34H, -CH₂-N-, -CH-, -CH₂-, ArCH₂ Ar, -OH, Ar-CH₂-N-), 4.23 (d, 4H, J= 19.6 Hz, ArCH₂ Ar), 6.33–6.86 (br, 10H, ArH). Anal. Calcd. For C₄₄H₅₈N₂ O₁₄; 62.99, C; 6.97, H; 3.34, N. Found: 63.02, C; 6.88, H; 3.32, N.

Synthesis of Calix 19 (5,11,17,23-tetra-tert-butyl-25,27-di(benzhydrazidylmetoxy)-26,28-dihydroxy-calix[4]arene): (Sayin and Yilmaz, 2011)

To a solution of dialkyl bromide of p-tert-butylcalix[4]arene (1.0 g, 1.12 mmol) in 40 mL of CH₃CN were added 0.7 g of K₂CO₃, 0.67 g of NaI, and benzhydrazide (2.53 g, 18.57 mmol), and the reaction mixture was stirred and heated under reflux. The reaction was monitored by using a TLC. After 4 days, the reaction mixture was filtered off, and the solvent was removed under reduced pressure. The residue was dissolved in 150 mL of CH₂Cl₂. The organic layer was extracted three times with water. The organic phase was dried (anhydrous MgSO₄); the solvent was removed under reduced pressure. In order to remove impurities, the crude product was precipitated by the addition of CH₃OH and filtered off. The solvent was evaporated and dried. A brown powder remained with 98 % yield, m.p.: (161 to 164)°C. The IR spectral data of 3 are (KBr disk) cm⁻¹: 1638(-NCd=O). ¹HNMR (400 MHz CDCl₃): δ 1.18 (s, 18H, Bu^t), 1.22 (s, 18H, Bu^t), 2.38-2.42 (m, 4H,-CH₂-), 3.37 (d, 4H,J =12.8 Hz, Ar-CH₂-Ar), 3.54-3.57 (m, 2H, -NH-), 3.76 (t, 4H, J = 6.8 Hz,-CH₂-), 4.18 (t, 4H,J = 4.8 Hz,-CH₂-), 4.29 (d, 4H, J = 12.8 Hz, Ar-CH₂-Ar), 7.01 (s, 4H, ArH), 7.06 (s, 4H, ArH), 7.39 (s, 2H,-OH), 7.47 (t, 4H,J = 7.2 Hz, ArH), 7.54 (t, 2H, J = 7.2 Hz, ArH), 7.88 (d, 4H, J = 8.0 Hz, ArH), 9.10 (s, 2H,-NH). Anal. Calcd for C₆₄H₈₀N₄O₆ (%): C, 76.77; H, 8.05; N, 5.60. Found (%); C, 76.94; H, 7.91; N, 5.77.

Since this research was supported by TUBITAK (Turkish Scientific Association) under project number TBAG 109T240, same name as in this project which are Calix 1, 4, 6, 8, 17, 18 and 19 were used for simplicity. Here, calix 1 was used as reference molecule due to the fact that it does not have any functional group and it was used to investigate the effect of functional groups on CO sensitivity. Two different compounds which contain iron molecules were used to dope calixarene molecules.

These compounds were iron (III) nitrate ($\text{Fe}(\text{NO}_3)_3 \cdot 9\text{H}_2\text{O}$) and iron (III) chloride ($\text{FeCl}_3 \cdot 6\text{H}_2\text{O}$). For simplicity, these iron-containing compounds were named as Fe(1) and Fe(2), respectively. First, solution of each bare calixarene was prepared in order to dope each calixarene molecule with iron. To prepare these solutions, 2.054 mg of Calix 6, 2.15 mg of Calix 8, 1.58 mg of Calix 17, 1.6 mg of Calix 18 and 1.66 mg of Calix 19 were solved in 5 ml of chloroform, respectively. After preparation of bare calixarene solutions, iron compounds were prepared to dope each calixarene molecule. That is, 4.1 mg of $\text{Fe}(\text{NO}_3)_3 \cdot 9\text{H}_2\text{O}$ compound was solved in 5 ml of ethanol. In addition, iron (III) chloride was already in liquid form. These prepared iron-containing solutions and bare calixarene solutions were mixed together in equal amount (0.5 ml) separately. This procedure has been done for each calixarene molecule. The Figure 3.14 shows solutions of bare calixarene, Fe(1) doped calixarene and Fe(2) doped calixarene molecule.

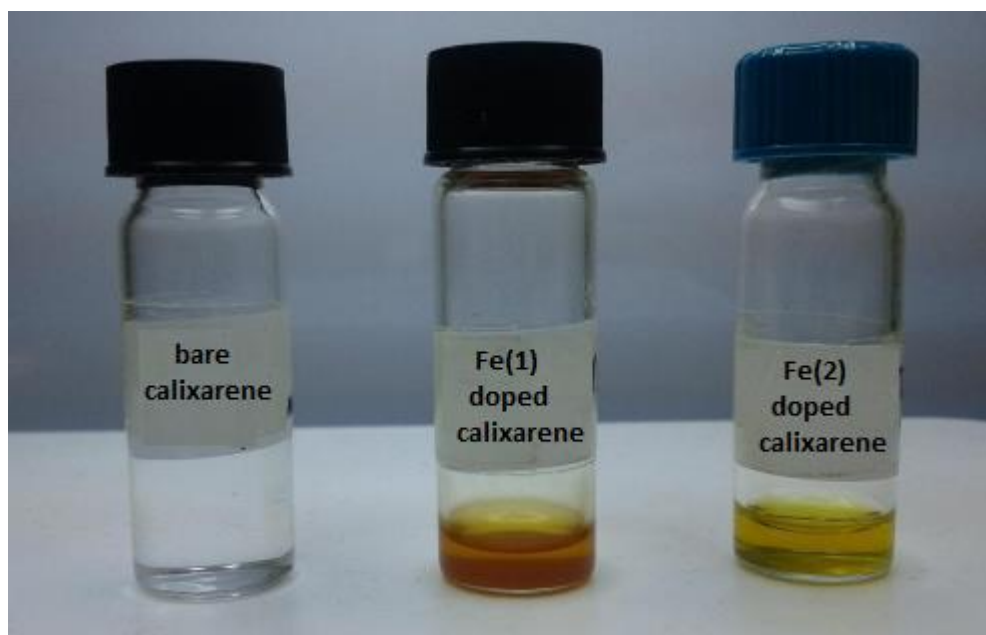


Figure 3.14. Bare calixarene, Fe(1) doped calixarene, Fe(2) doped calixarene

As to preparation of QCM electrodes, this process starts with cleaning procedure. To do this, the following procedure was performed. QCM electrodes were rinsed in acetone, ethanol, propanol and distilled water in ultrasonic cleaner for 15 minutes, respectively. Finally, nitrogen was used to dry QCM electrodes as a final step of cleaning, as given in Figure 3.15.

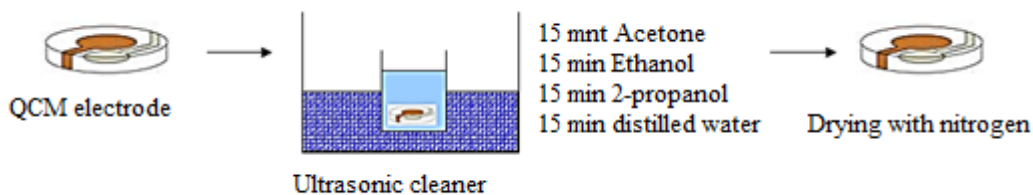


Figure 3.15. Cleaning of QCM electrodes

After the cleaning procedure, the resonant frequency of QCM electrodes was obtained, using CHI400 instruments (F_0). Then, 5 μ l of each of previously prepared iron doped and bare calixarene solutions were dropped on cleaned QCM electrodes, using micropipette. Afterwards, the electrodes were kept at 60°C for one hour.

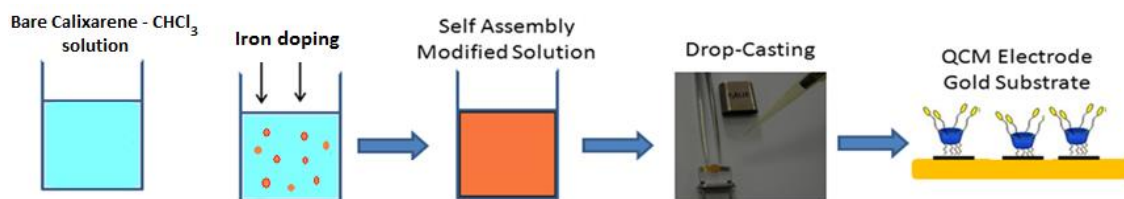


Figure 3.16. Preparation of thin films on QCM using drop-casting technique

After preparation of thin films, the resonant frequency of each QCM electrodes was measured. (F_1) The measured frequency values before and after dropping of each solution were used to determine the mass loaded on QCM electrodes so that the sensitivity of each film to CO gas could be investigated. The mass of each thin film loaded on QCM electrodes, resulted in a frequency shift, was used as normalization constant in investigation of sensitivity of doped and undoped calixarene molecules to CO gas.

CHAPTER 4

RESULTS AND DISCUSSIONS

This chapter contains two parts including QCM results and electrical results of iron doped and undoped calixarene molecules. In the first part,, CO sensing properties of iron doped and undoped calixarene molecules under exposure of CO molecules with different concentration are presented by using QCM technique. In order to investigate the sorption kinetics of all molecules, Langmuir model has also been used and the results are given in this section. Furthermore, three dimensional structures and dipole moments of undoped calixarene molecules, calculated by Prof Dr. Mustafa Kurt from Ahi Evran University, have been given. Finally, electrical responses of CNT added and iron doped calixarene molecules are presented.

4.1. Investigation of CO Gas Sorption Kinetics of Molecules by Using QCM Method

In this study, the CO gas adsorption and desorption kinetics of iron doped and undoped functional calixarene molecules is investigated using QCM technique for both dry air and nitrogen that are used as desorption gases. The aim of using dry air as desorption gas as well as high purity nitrogen is to investigate CO selectivity of all calixarene molecules in air environment. The gas flow rates for both desorption and adsorption gases were 500 sccm (standard cubic centimetre per minute). In this section, comparative results of CO gas adsorption and desorption kinetics of thin film of iron doped and undoped functional calixarene molecules are given. In the present study, CO gas will be considered as active gas for simplicity. Firstly, the maximum and minimum active gas was sent to the test cell for two periods of time. That is, the desorption gas (nitrogen or dry air) was first sent to the test cell for 200 s for cleaning process of both environment and surface of thin film and then the active gas (CO) was sent for 100 s for adsorption process. Afterwards, desorption gas was resent to the test cell to start desorption process. Then, the same process was done one more time to see if the results

were repeatable and the test was completed. This is called this as periodic measurement.

The recipe of periodic measurement is given below and in Figure 4.1

The steps for periodic measurement are;

- 0-200s: N₂ or dry air (500 sccm)
- 200-300s: active gas (500 sccm)
- 300-500s: N₂ or dry air (500 sccm)
- 500-600s: active gas (500 sccm)
- 600-700s: N₂ or dry air (500 sccm)

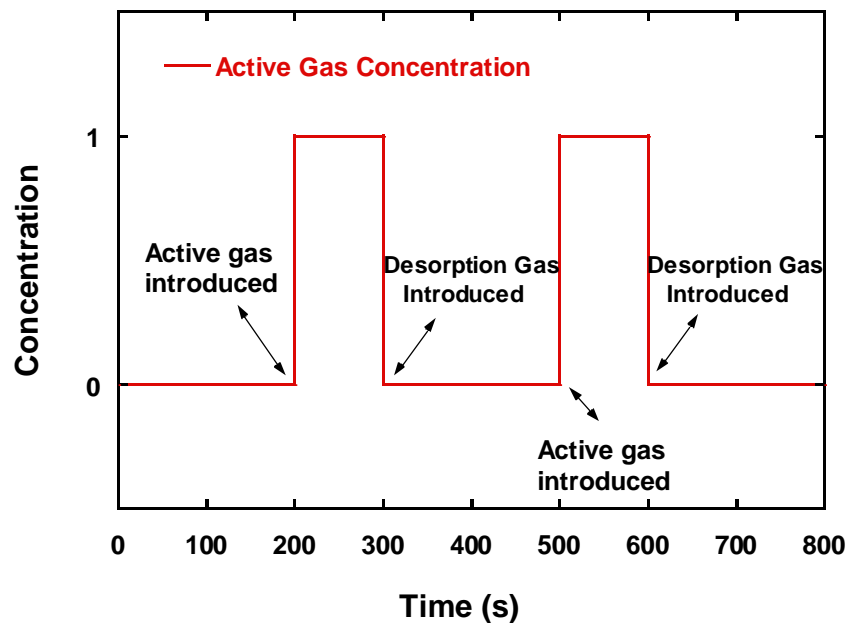


Figure 4.1. Steps of periodic measurement

The present study investigates the variations in frequency shift of iron doped and undoped calixarene coated QCM crystals with different concentrations in addition to periodic measurement. The CO level was increased by 10 sccm steps for equal time intervals of 5 s and then CO level was decreased by 10 sccm steps for equal time intervals of 10 s, in order to investigate the linear responses of all molecules, as seen in Figure 4.2. CO gas with a concentration of 10000 ppm (parts per million) was used in this study.

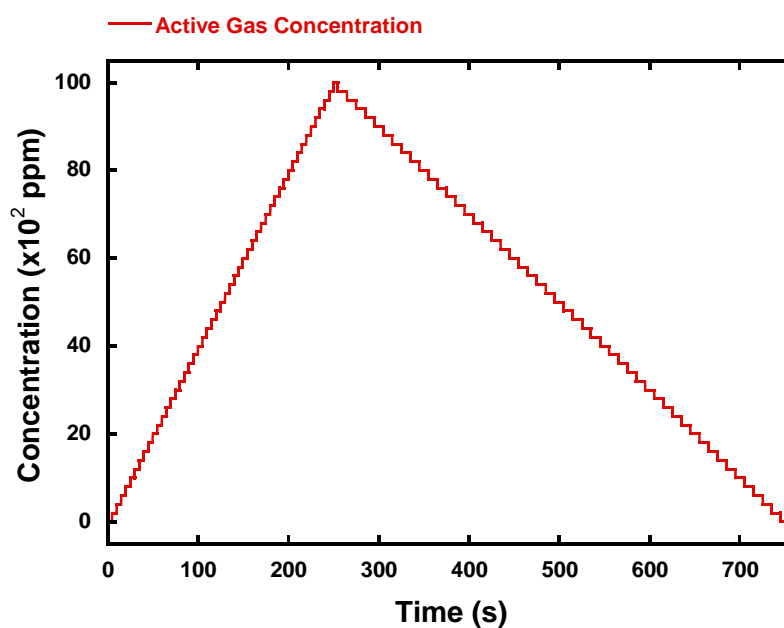


Figure 4.2. Steps of linear measurement

By analysing of the data obtained from periodic and linear measurements (frequency shift, ΔF), the plots illustrating the sensitivities of all calixarene molecules to CO gas for both nitrogen and dry air, used as desorption gases separately, have been obtained. The sensitivity of each molecule to CO has been defined as ratio of the mass of gas molecules adsorbed on the surface of molecule coated on QCM (Δm) to the mass of coated film (Δm_0) per thousand. As it was mentioned in Chapter 3, a net change of 1 Hz corresponds to 1.34 ng of gas molecules adsorbed or desorbed onto the crystal surface. Hence, Δm can be found by multiplying ΔF values, obtained during measurements, with 1.34. Likewise, Δm_0 can be found by multiplying the frequency shift before and after coating QCM electrode with 1.34. Therefore, the equation giving the sensitivity is calculated as following;

$$Sensitivity = \frac{\Delta m}{\Delta m_0} \times 1000$$

where Δm and Δm_0 are;

$$\Delta m = \Delta F \times 1,34 \text{ ng}$$

$$\Delta m_o = (\Delta F_o) \times 1,34 \text{ ng}$$

Substituting Δm and Δm_o into sensitivity equation will be in the following form;

$$\text{Sensitivity} = \frac{\Delta F}{\Delta F_o} \times 1000$$

4.1.1. Investigation of CO Gas Sorption Kinetics of all Calixarene Molecules by Using QCM Method

The adsorption and desorption kinetics of each molecule have been investigated according to the functional group of each of calixarene molecule. As it has been stated in Chapter 1, the functional groups at the upper and lower rims determine selectivity in host-guest interactions and physical properties of calixarene molecules (Kocabas et al., 2006; Ohira et al., 2009). Physical properties of calixarene molecules are dependent on the lower rim functional groups. What is more, the apolar cup-shaped cavity adsorbs and desorbs guest molecule which determines the zeolite-like behaviour of calixarenes at the nano-scale (Filenko et al., 2005). Hence, each of the calixarene molecules having different functional group has shown different affinity to CO gas molecules. Furthermore, in this thesis study, calix 1 was taken as reference molecule which does not have any functional group compared to others. The functional groups in the other used calixarene molecules are slightly different from each other. Since these functional groups are polar, it is expected that they will interact with active gas due to unequal charge distribution.

On the other hand, conformation of calixarenes is one of the most important factors that affect the dipole moments of calixarene molecules (Demendoza et al., 1993; Kelderman et al., 1992). Variable conformations in calixarenes are caused by the rotations of the methylene groups between phenols. These molecules often exist in the cone, partial cone, 1,2-alternate, or 1,3-alternate conformation as stated before (Gutsche et al., 1983). In this study, it was clearly seen that functionalizing calixarene molecules with different functional group changed the dipole moments and structure of calixarene

Table 4.2 (cont.)

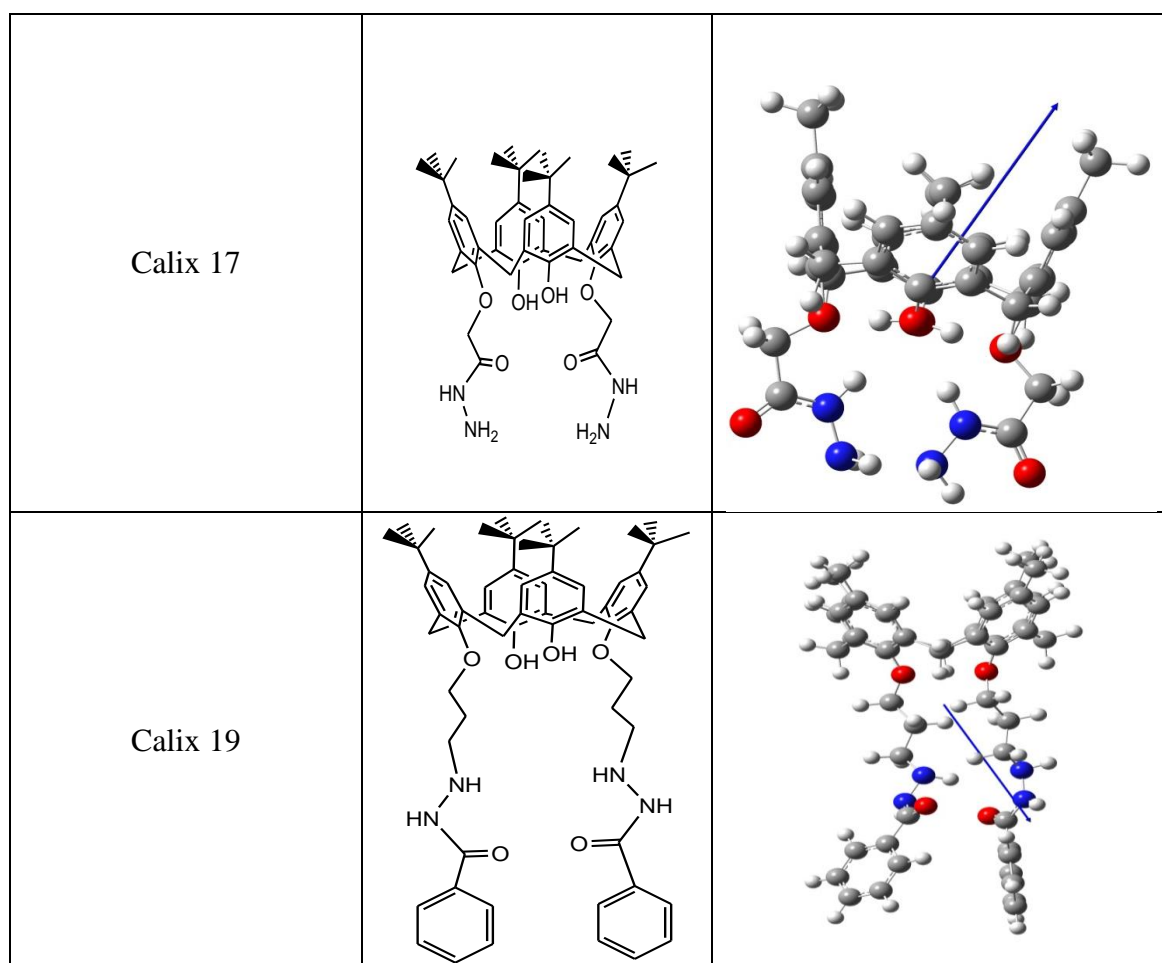


Table 4.3. Dipole moments of calixarene molecules

Molecule	Dipole Moment Components (Debye)			Total dipole moment (Debye)
	μ_x	μ_y	μ_z	μ_{total}
Calix 1	1.44	6.50	1.03	6.74
Calix 6	0.29	-1.45	-0.45	1.55
Calix 8	-3.11	0.84	3.76	4.94
Calix 17	0.63	-7.79	-1.57	7.97
Calix 19	-2.26	-1.15	-0.23	2.55

In this study, the responses of six different functional calixarene molecules coated on QCM electrodes to CO gas were investigated. First, sorption kinetics of bare calixarene molecules was investigated according to procedure explained in Chapter 3. That is, the thin films of undoped calixarene molecules on QCM electrodes were prepared using drop-casting method and response of each of them to CO were investigated. Figure 4.3 show the responses of all undoped calixarene molecules under exposure of CO gas for comparison. In addition, maximum response of each molecule is given in Table 4.4 in the order from the largest to the smallest.

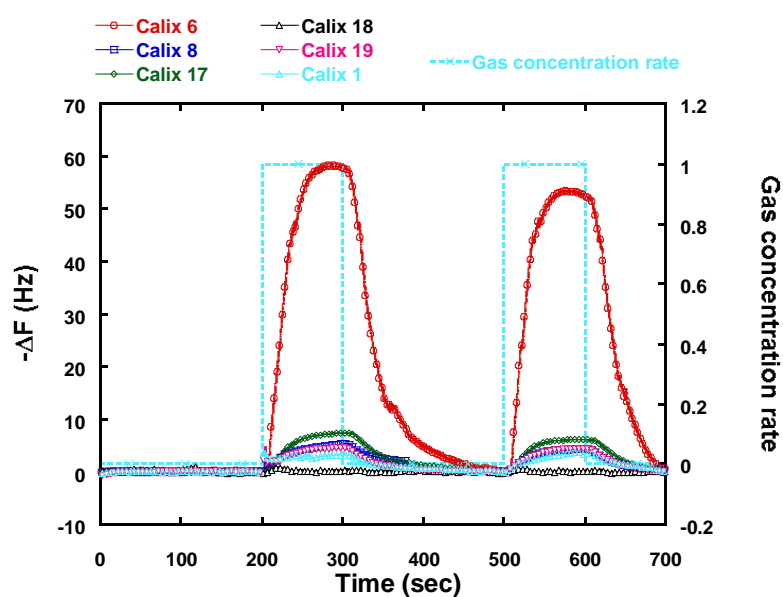


Figure 4.3. Periodic responses of all various functional calixarene molecules to CO

Table 4.4. Maximum response of each undoped calixarene molecules to CO

Molecule	ΔF_{\max} (Hz)
Calix 6	58.3
Calix 17	7.36
Calix 8	5.27
Calix 19	4.58
Calix 1	3.2
Calix 18	0.83

As stated in Chapter 3, there are two different complexes which contain iron molecules used to dope each calixarene molecule. One of them is iron (III) nitrate ($\text{Fe}(\text{NO}_3)_3 \cdot 9\text{H}_2\text{O}$) and the other one is iron (III) chloride ($\text{FeCl}_3 \cdot 6\text{H}_2\text{O}$). For simplicity, the first one (iron III nitrate) is named as Fe(1) while the latter one is Fe(2). Furthermore, iron doped calixarene molecules are named as in the form of Calix #_Fe(#).

After investigation of bare calixarene molecules, CO sorption kinetics of Fe(1) doped calixarene molecules were studied and QCM electrodes were prepared according to procedure explained in Chapter 3. Figure 4.4 shows the comparative responses of all Fe(1) doped calixarene molecules (Calix #_Fe(1)) under exposure of CO gas. Furthermore, Table 4.5 shows the maximum responses of them to CO in the order from the largest to the smallest.

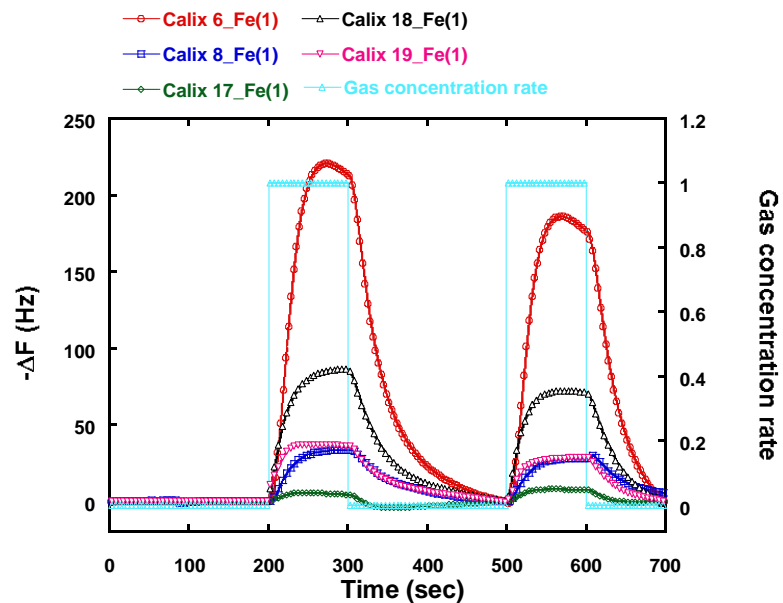


Figure 4.4. Periodic responses of Fe(1) doped calixarene molecules to CO

Table 4.5. Maximum responses of Fe(1) doped calixarene molecules to CO

Molecule	ΔF_{\max} (Hz)
Calix 6_Fe(1)	220.7
Calix 18_Fe(1)	86.14
Calix 19_Fe(1)	35.76
Calix 8_Fe(1)	32.99
Calix 17_Fe(1)	5.54

Finally, the CO gas sensing capabilities of Fe(2) doped calixarene molecules (Calix #_Fe(2)) coated on QCM electrodes have been investigated. The results of them are displayed in Figure 4.5 for comparison. In addition, maximum responses of them to CO are given in Table 4.6 in the order from largest to smallest.

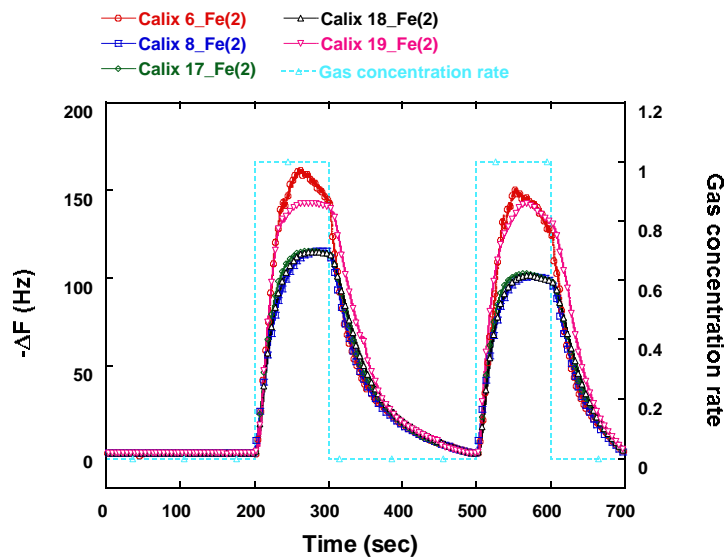


Figure 4.5. Periodic responses of Fe(2) doped calixarene molecules to CO

Table 4.6. Maximum responses of Fe(2) doped calixarene molecules to CO

Molecule	ΔF_{\max} (Hz)
Calix 6_Fe(2)	161.36
Calix 19_Fe(2)	142.67
Calix 8_Fe(2)	115.4
Calix 17_Fe(2)	115.2
Calix 18_Fe(2)	114.9

The bar graph, in Figure 4.6, illustrates the maximum response of all iron doped and undoped calixarene molecules. This plot has been given to be able to compare all of the results.

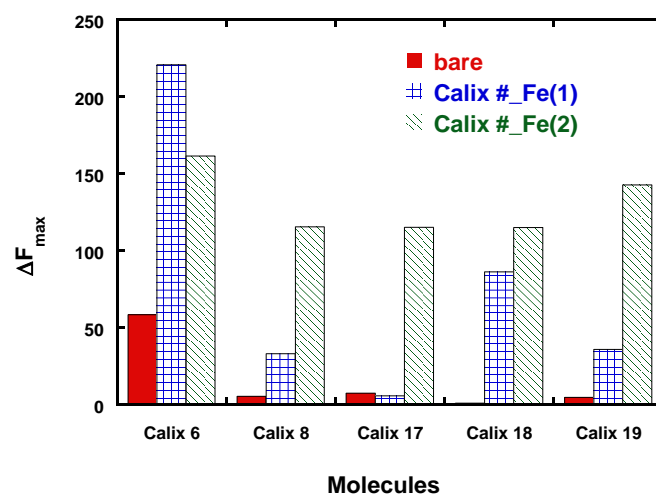


Figure 4.6. Bar graphs illustrating maximum responses of all molecules to CO

In addition to investigation of the frequency shift response of all iron doped and undoped molecules coated on QCM electrodes, the sensitivity of each prepared molecule to CO was investigated. To do this, sensitivity graphs of each calixarene molecule has been obtained according to the calculations given above. In other words, the QCM results given above was used to obtain sensitivity of all molecules to CO gas. The ΔF_0 and corresponding Δm_0 values, needed to convert frequency shift values into sensitivity, for each calixarene molecule are presented in Table 4.7.

Table 4.7. ΔF_0 and Δm_0 (μg) values of all molecules

Molecule	ΔF_0 (Hz)	Δm_0 (μg)
Calix 1	9085	12.2
Calix 6	11295	15.1
Calix 8	5662	7.58
Calix 17	10727	14.3
Calix 18	6106	8.2
Calix 19	6807	9.1
Calix 6_Fe(1)	5088	6.8
Calix 8_Fe(1)	4999	6.7
Calix 17_Fe(1)	453	0.6
Calix 18_Fe(1)	3087	4.1
Calix 19_Fe(1)	943	1.3
Calix-6_Fe(2)	7701	10.3
Calix-8_Fe(2)	2969	3.98
Calix 17_Fe(2)	20005	26.8
Calix 18_Fe(2)	13083	17.5
Calix 19_Fe(2)	12640	16.9

In order to obtain sensitivity plots of all molecules, all frequency shift values were multiplied by 1000 and then divided by ΔF_0 and the results for all iron doped and undoped calixarene molecules were plotted.

After the calculation of the sensitivities of each bare calixarene molecule to CO gas, the following plot was obtained. (Figure 4.7). Added to this, maximum sensitivities of each undoped calixarene molecules are given in Table 4.8 in the order from the largest to the smallest.

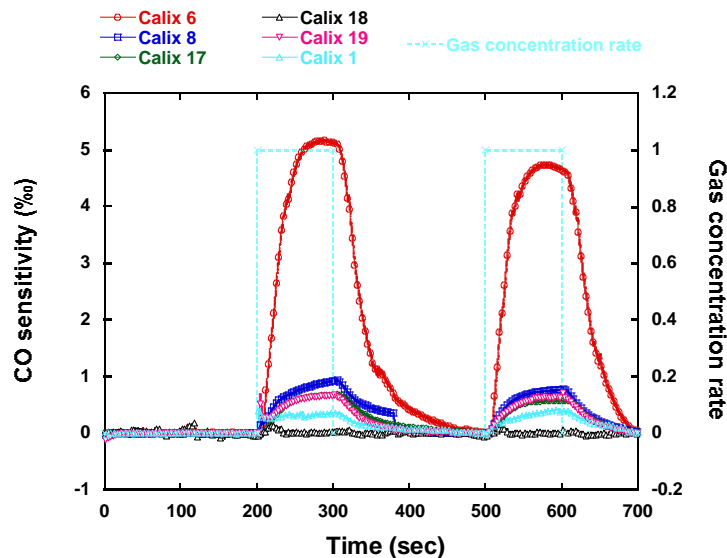


Figure 4.7. Sensitivities of bare calixarenes to CO

Table 4.8. Maximum sensitivities of each undoped calixarene molecules to CO

Molecule	CO sensitivity
Calix 6	5.16
Calix 8	0.93
Calix 17	0.69
Calix 19	0.66
Calix 1	0.35
Calix 18	0.12

As seen in Table 4.8, Calix 6, functionalized with four pyridine groups, shows highest affinity to CO molecules compared to other calixarene molecules. Looking at three dimensional picture of Calix 6, it is seen that two pyridine groups are quite near to each other, while the others look far from each other. Such a high sensitivity may stem from dipole-dipole interaction between CO and nitrogen atom in the pyridine groups. In addition, affinity of calix 18 to CO is less than others. According to the molecular structure of Calix 18, it is seen that it is functionalized with hydroxyl groups and methyl

glucamine groups. These groups will give rise to steric effect and do not let CO molecules to get into the active sites of calix 18. Furthermore, because hydroxyl groups have a potential to make hydrogen bond with each other, this will decrease the polar interactions between CO and functional groups. The same effect can also be seen for calix 1 because of hydroxyl groups from lower rims. In addition, it is seen that functionalization of calixarene increased the affinity to CO.

Similarly, Figure 4.8 illustrates the comparative sensitivities of Fe(1) doped calixarene molecules to CO gas and maximum sensitivities of them are given in Table 4.9 in the order from largest to smallest.

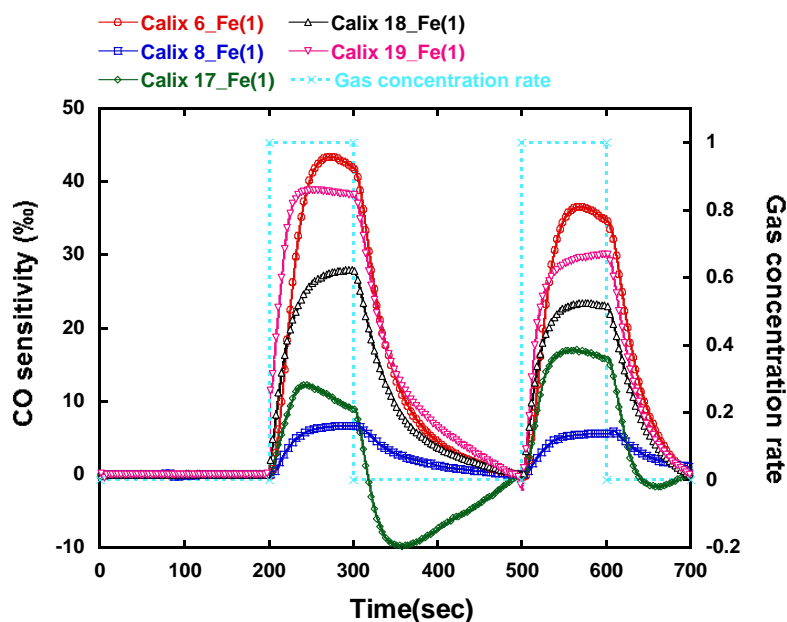


Figure 4.8. Sensitivities of Fe(1) doped calixarenes to CO

Table 4.9. Maximum sensitivities of each Fe(1) doped calixarene molecules to CO

Molecule	CO sensitivity
Calix 6_Fe(1)	43.38
Calix 19_Fe(1)	38.83
Calix 18_Fe(1)	27.88
Calix 17_Fe(1)	12.16
Calix 8_Fe(1)	6.57

Table 4.9 shows that there is a remarkable increase in the affinity of calixarene to CO up to 200 times compared to bare calixarene molecules after Fe(1) doping. That is, while the maximum response of calix 18 to CO is 0.12, it becomes 27.88 when doped with Fe(1).

Finally, the sensitivities of Fe(2) doped calixarene molecules to CO have been investigated and the results are illustrated in Figure 4.9. In addition, maximum responses of them to CO are shown in Table 4.10 in the order from largest to smallest.

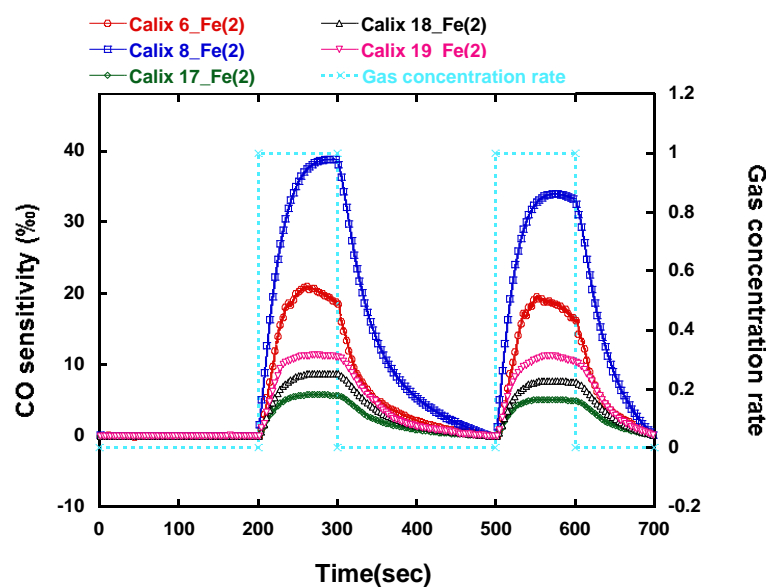


Figure 4.9. Sensitivities of Fe(2) doped calixarenes to CO

Table 4.10. Maximum sensitivities of each Fe(2) doped calixarene molecules to CO

Molecule	CO sensitivity
Calix 8_Fe(2)	38.89
Calix 6_Fe(2)	20.94
Calix 19_Fe(2)	11.27
Calix 18_Fe(2)	8.78
Calix 17_Fe(2)	5.76

According to the Table 4.10, doping of calixarene molecules with Fe(2) increased the sensitivities of them to CO compared to bare calixarene molecules. However, if the results of Fe(1) doped calixarenes with Fe(2) doped ones are compared, it is clearly seen that the order changed. For instance, while calix 8_Fe(1) shows least sensitivity to CO compared to other Fe(1) doped calixarenes, it becomes the most sensitive one when doped with Fe(2) compared to other Fe(2) doped calixarenes. If the responses of Fe(2) doped calixarenes with Fe(1) doped ones are compared, it is seen that doping calixarenes with iron (III) nitrate made calixarene more sensitive to CO compared to iron (III) chloride doped calixarenes. This may be due to the fact that chloride ion (Cl^-) is bigger than that of nitrate ion (NO_3^-) in terms of volume and this may cause steric effect. If we compare the molecular structure of calix 6,19 and 8 which are quite sensitive to CO, it is seen that they have similar molecular structure. Furthermore, since NH groups in alkyl chains, possibly bond to iron atoms, does not have a molecular geometry causing steric effect, CO atoms can easily interact with Fe atoms in the centre and increase the sensitivity. To be able to see comparison of the sensitivity results of all molecules, the bar graph has been plotted as seen in Figure 4.10.

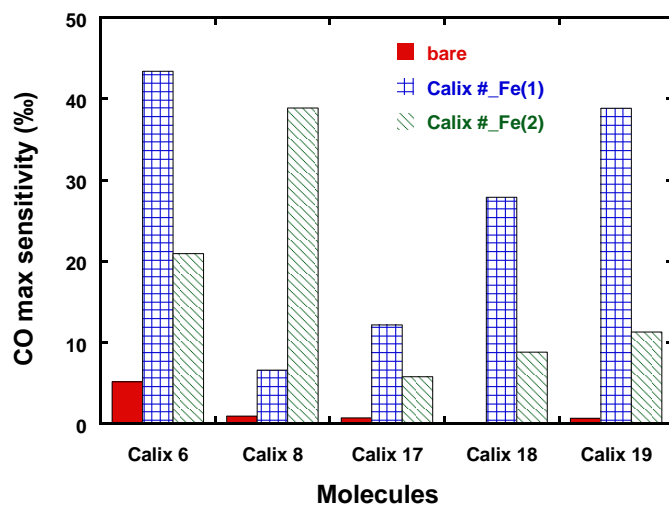


Figure 4.10. Bar graph showing maximum sensitivities of all molecules

As stated above, the linear responses of all molecules to CO were investigated and the results are given in the following figures.

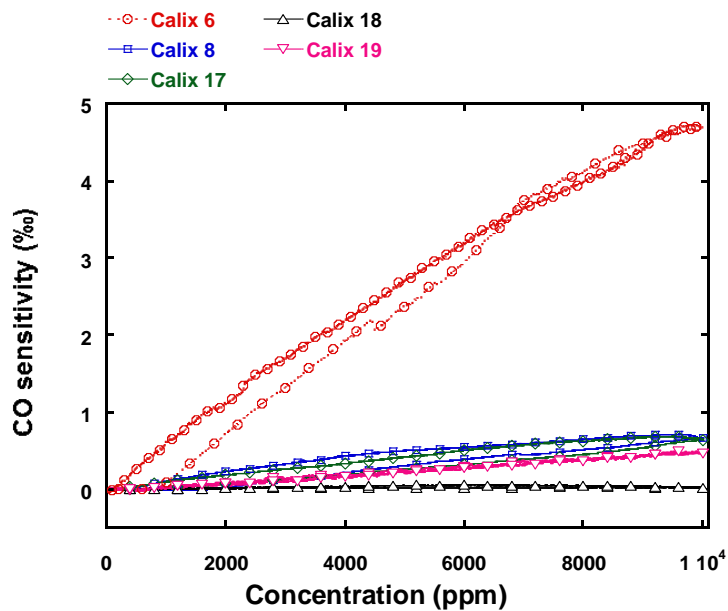


Figure 4.11. Linear responses of bare calixarenes to CO

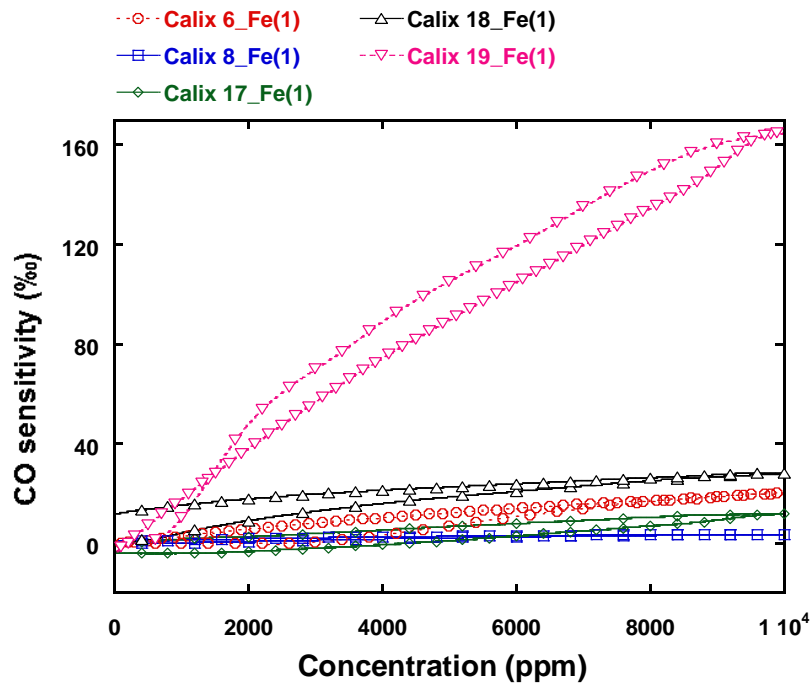


Figure 4.12. Linear responses of Fe(1) doped calixarenes to CO

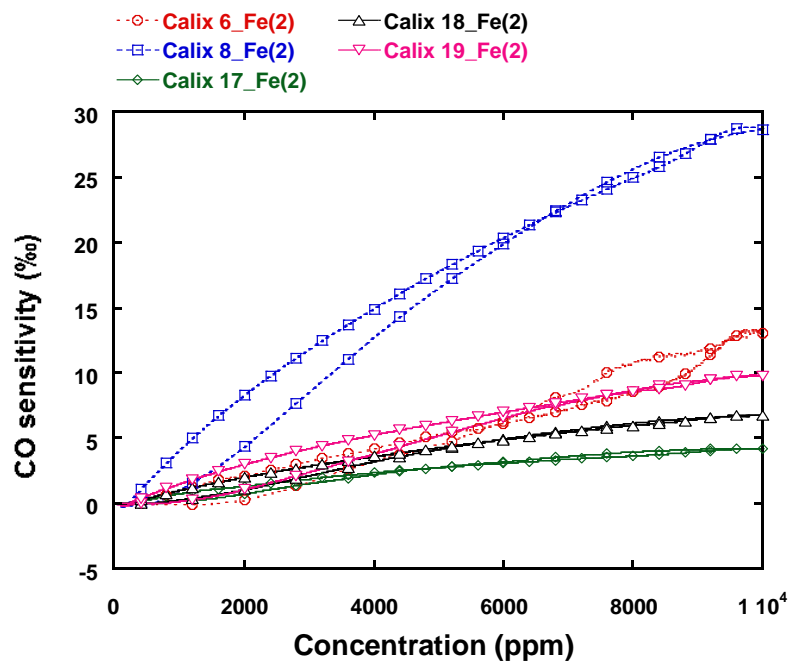


Figure 4.13. Linear responses of Fe(2) doped calixarenes to CO

In addition to analysis of sensitivities of all molecules to CO in N₂ environment, the CO sensitivities of all of them were investigated in air environment. The results are illustrated in following figures.

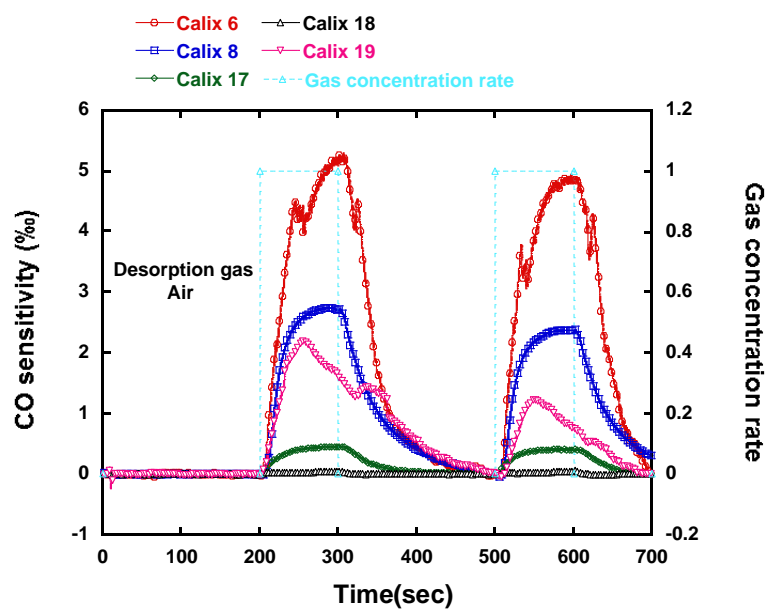


Figure 4.14. CO sensitivities of bare calixarenes in air environment

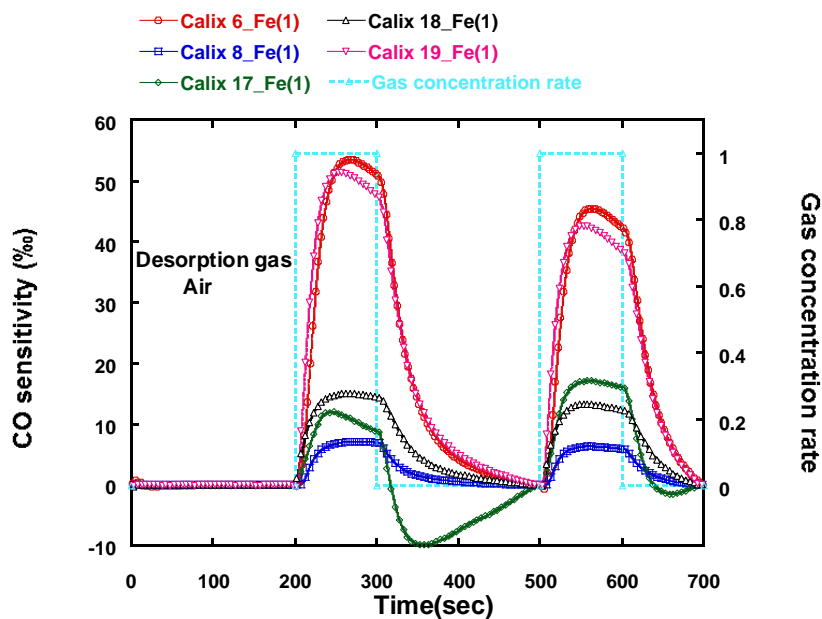


Figure 4.15. sensitivities of Fe(1) doped calixarenes in air environment

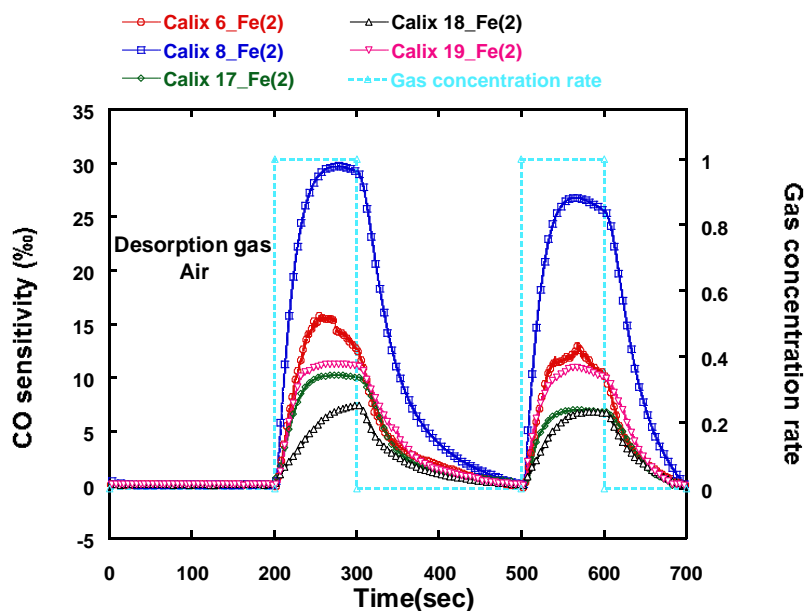


Figure 4.16. sensitivities of Fe(2) doped calixarenes in air environment

Table 4.11. Maximum responses of all molecules in both air and N₂ environment

Molecules	Max response in air environment	Max response in N ₂ Environment
Calix 6	5.10	5.16
Calix 8	2.72	0.93
Calix 17	0.46	0.69
Calix 18	0.06	0.12
Calix 19	2.21	0.66
Calix 6_Fe(1)	53.20	43.38
Calix 8_Fe(1)	7.280	6.57
Calix 17_Fe(1)	11.86	12.16
Calix 18_Fe(1)	14.86	27.88
Calix 19_Fe(1)	51.50	38.83
Calix 6_Fe(2)	15.45	20.94
Calix 8_Fe(2)	29.86	38.89
Calix 17_Fe(2)	10.20	5.76
Calix 18_Fe(2)	7.410	8.78
Calix 19_Fe(2)	11.25	11.27

As seen in Table 4.11, there is no remarkable change in sensitivities of each molecule when the experiments were carried out in air environment. There has been small decrease in the sensitivity for each molecule to CO in air environment which may be due to the fact that air includes some other active gases like O₂ and CO₂ which may have occupied the active sites on the surface of molecules.

All in all, there are many factors affecting the sensitivity of all molecules to CO. One of them is conformational structure of molecules which are given in Table 4.1. (DFT; three dimensional structures of molecules) That is, if the molecular structure of calixarene is suitable to interact with iron molecules, then the sensitivity of the related molecule to CO will increase. More clearly, the more iron exist in molecule, the more sensitive it will be. For example, it is seen in Table 4.1 that calix 6 seems to have three baskets which will give rise to possibility of more place for iron molecule that will increase the affinity of calix 6_Fe(1) to CO. On the other hand, calix 17 seems to have only one basket which result in less amount of iron molecule in calix 17. Hence, the sensitivity of calix 17_Fe(1) is small compared to other Fe(1) doped calixarenes. The other factor is that Fe⁺³ has binding affinity to OH-carbonyl and amino groups.(Burke et al., 2000; Nawara et al., 2013; Ochiai et al., 2012) That is, existence of these functional groups will decrease the binding affinity to CO. More clearly, this interaction will decrease the CO binding capacity of Fe⁺³ which has a potential to bind to six CO molecules. For example, calix 8_Fe(1) showed less affinity to CO compared to others which may be because it has OH and carbonyl groups. Calix 18_Fe(2) also showed less affinity to CO compared to other molecules which may be due to the fact that it has hydroxyl, carbonyl and amino groups.

4.1.2. Investigation of Adsorption and Desorption Kinetics of all Molecules with Langmuir Adsorption Model

In order to analyse the obtained frequency shift results and sensitivity results, Langmuir adsorption model has also been used. This model is frequently used to describe adsorption kinetics of CO gas molecules onto organic or inorganic films(Karpovich and Blanchard, 1994). According to Langmuir adsorption isotherm model, the rate of surface reaction to form a monolayer on the surface is given with the following equations:

$$\frac{d\theta}{dt} = k_a(1-\theta)C - k_d\theta \quad (1)$$

Here, θ is a unitless quantity, which express the fraction of surface coverage, C is the gas concentration, k_a and k_d are the adsorption and desorption constants, respectively. Integration of Eq. (1) leads to:

$$\theta(t) = K'(1 - e^{-k_{ads}t}) \quad (2)$$

where k_{ads} is the inverse of the relaxation time and K' is the association constant defined as following;

$$K' = \frac{k_a C}{k_a C + k_d} \quad \text{and} \quad k_{ads} = k_a C + k_d \quad (3)$$

Here, QCM has been used to measure the fractional coverage as a function of time during the adsorption of CO molecules by various functional bare and iron doped Calixarene molecules, and the increase in the frequency shift reflects the molecular mass uptake or loss. Thus the difference between the oscillation frequency shift (ΔF) of coated and uncoated QCM is directly proportional to the adsorbed mass of CO molecules. The relationship between the surface adsorption kinetics and frequency shift (ΔF) of QCM can be expressed as following;

$$\Delta f(t) = \Delta f_{\max} K'(1 - e^{-k_{ads}t}) \quad (4)$$

Using Sauerbrey relation, ($\Delta m = -(1.34\text{ng/Hz})\Delta f$), the time dependent variation of mass of the adsorbed CO molecules on all iron doped and iron doped calixarene film surface Δm_t can be defined as:

$$\Delta m_t = \Delta m_{\infty} (1 - e^{-t/\tau}) \quad (5)$$

$$\tau^{-1} = k_a \times C[\text{CO molecules}] + k_d \quad (6)$$

Δm_{∞} is the maximum amount of adsorbed CO molecules on the surface for $\tau \rightarrow \infty$ and τ is the relaxation time.

With the help of Langmuir isotherm adsorption model, the details of which is given above, the CO adsorption and desorption kinetics of all iron doped and undoped calixarene molecules are analysed. In order to utilize this model, the frequency shift versus time (ΔF -t) plots has been plotted again as mass adsorbed on thin film surface on QCM versus time by only multiplying frequency shift axis by 1.34 ng/Hz.

Figure 4.17-19 illustrate the adsorbed mass by surface of thin film of all calixarene molecules versus time.

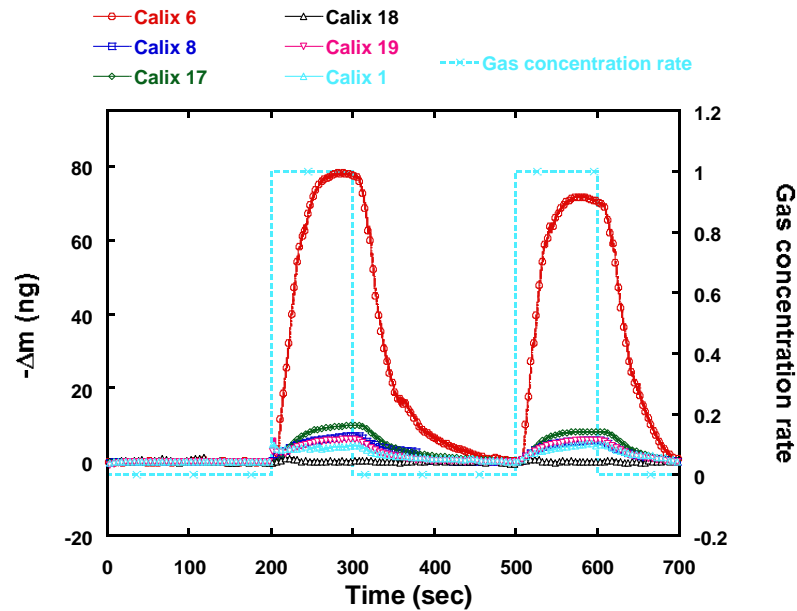


Figure 4.17. Adsorbed mass on the surface of bare calixarene molecules versus time

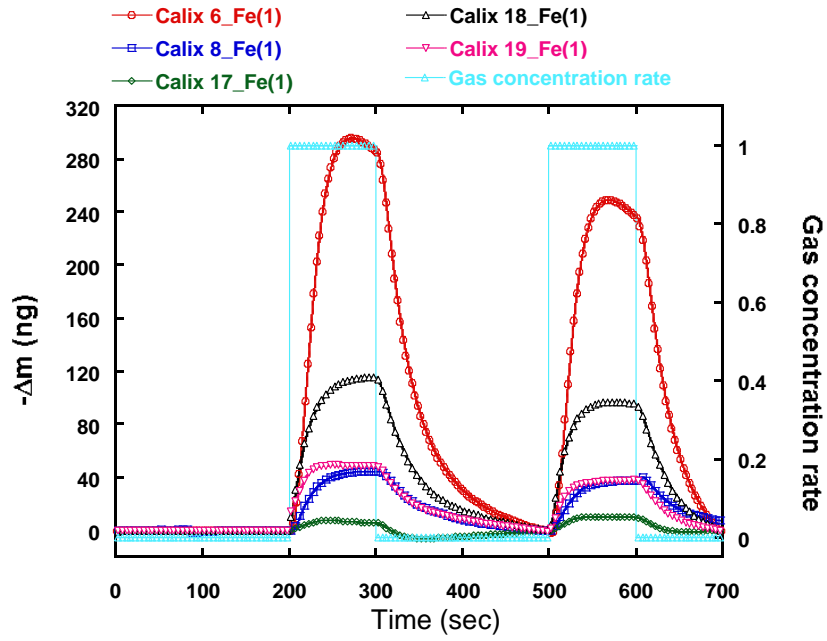


Figure 4.18. Adsorbed mass on the surface of Fe(1) doped calixarene molecules versus time

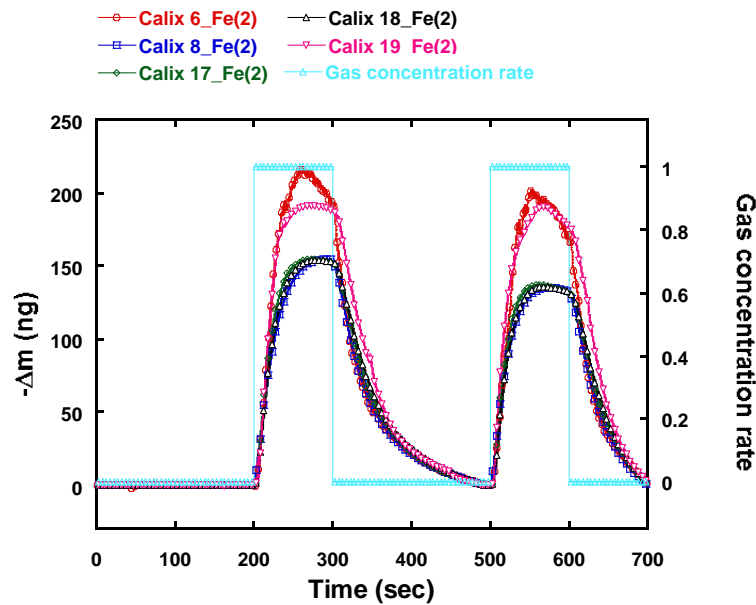


Figure 4.19. Adsorbed mass on the surface of Fe(2) doped calixarene molecules versus time

Figure 4.20, obtained by using Figure 4.17, illustrates the least square fits (solid lines) using Langmuir adsorption isotherm model given in equation (5) for adsorption parts of the data for 10000 ppm CO gas concentration for thin films of bare calixarene molecules coated on QCM.

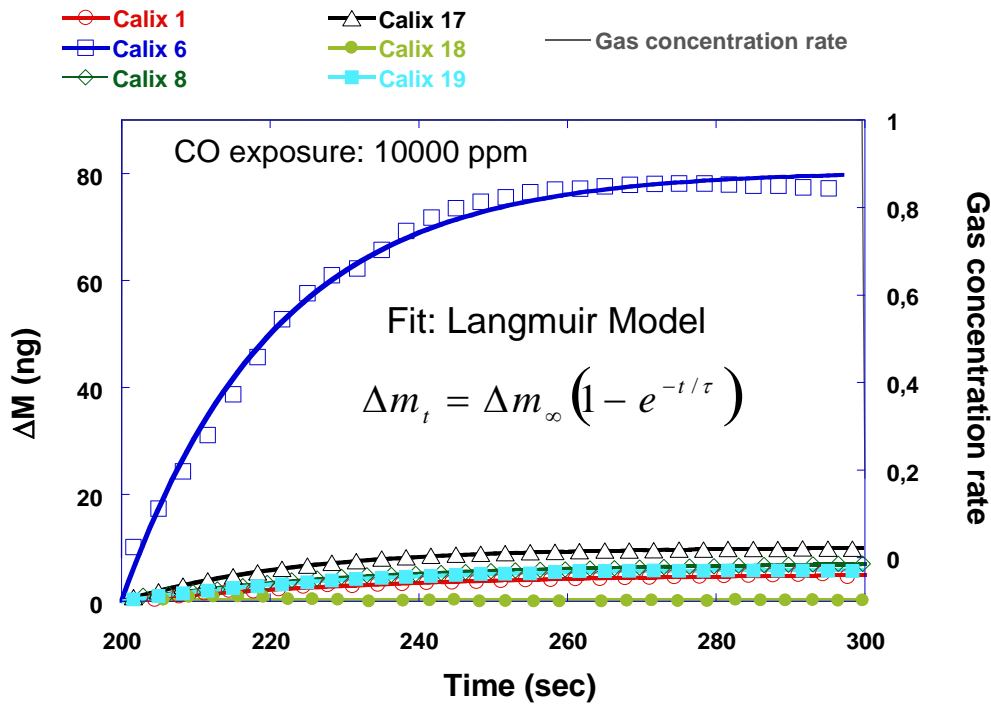


Figure 4.20. QCM results of bare calixarenes: the least square fit (solid lines) using the Langmuir adsorption isotherm model given in Equation (5) for 10000 ppm CO concentration

Similarly, Figure 4.21, obtained by using Figure 4.18, shows the least square fits (solid lines) using Langmuir adsorption isotherm model for adsorption parts of the data for 10000 ppm CO gas concentration for thin films of Fe(1) doped calixarene molecules.

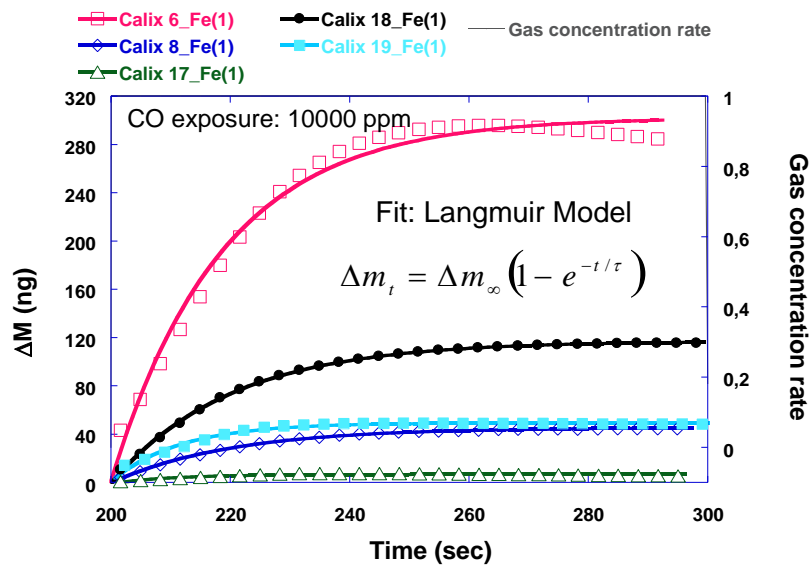


Figure 4.21. QCM results of Fe(1) doped calixarenes: the least square fit (solid lines) using the Langmuir adsorption isotherm model given in Equation (5) for 10000 ppm CO concentration

Finally, the least square fits (solid lines) obtained by using Langmuir adsorption isotherm model for adsorption parts of the data for 10000 ppm CO gas concentration for thin films of Fe(2) doped calixarene molecules are given in Figure 4.22, obtained by using Figure 4.19.

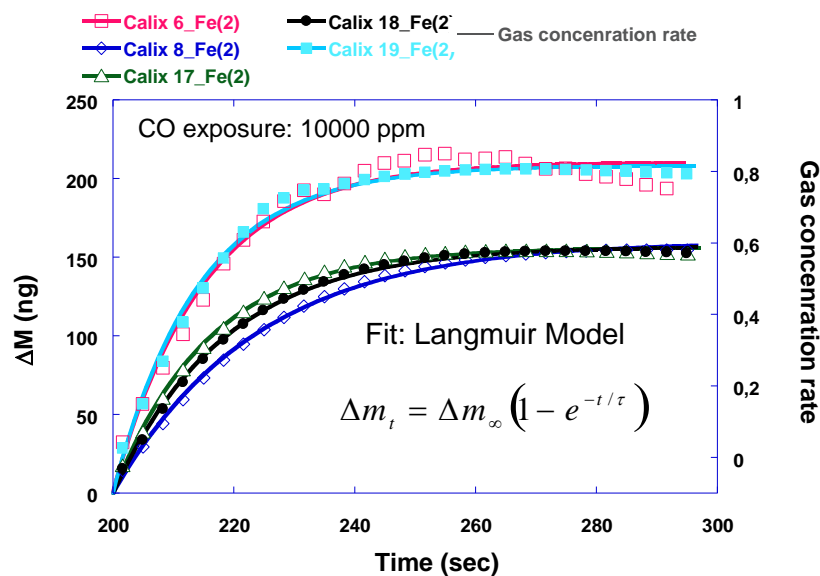


Figure 4.22. QCM results of Fe(2) doped calixarenes: the least square fit (solid lines) using the Langmuir adsorption isotherm model given in Equation (5) for 10000 ppm CO concentration

From the least square fit to the Equation (5), the relaxation times of the each adsorption process were calculated and given in Table 4.12 for all bare calixarenes and iron doped calixarenes, respectively. In addition, the response time at %90 of the maximum absorbed mass in Figure 4.17-19 were obtained and given in Table 4.12 for all molecules. Furthermore, Δm_{∞} is the maximum amount of adsorbed CO molecules on the surface for $t \rightarrow \infty$ and τ is the relaxation time, given in Table 4.12.

Table 4.12. Langmuir fit results

Molecules	Δm_{∞} (ng)	τ (s)	K_a	K_d	Response Time (s)	Recovery Time (s)
Calix 1	5.4989	38.12	2.503	0.0012	37.21	154.0
Calix 6	84.364	20.60	4.624	0.0023	49.31	91.70
Calix 8	7.4735	32.14	2.971	0.0014	69.31	83.21
Calix 17	10.63	22.80	4.185	0.0020	59.51	129.0
Calix 19	6.498	27.64	3.448	0.0017	56.51	80.00
Calix 6_Fe(1)	316.74	18.58	5.131	0.0025	45.50	101.4
Calix 8_Fe(1)	48.119	20.07	4.743	0.0024	46.7	132.2
Calix 17_Fe(1)	7.968	10.79	8.83	0.0044	30.4	14.7
Calix 18_Fe(1)	123.889	20.11	4.731	0.0024	44.6	116.4
Calix 19_Fe(1)	50.877	11.73	8.123	0.0040	23.7	132.02
Calix-6_Fe(2)	220.26	15.03	6.34	0.0031	43.31	101.32
Calix-8_Fe(2)	168.55	23.69	4.02	0.0020	48.21	117.4
Calix 17_Fe(2)	164.43	15.94	5.98	0.0029	37.4	117.72
Calix 18_Fe(2)	165.50	18.48	5.16	0.0025	42.71	125.52
Calix 19_Fe(2)	218.46	14.14	6.74	0.0033	32.8	110.52

4.2. Electrical Results

Electrical properties of all molecules under exposure of CO have been investigated by using interdigitated electrodes. The recipe of periodic measurement for investigation of electrical properties is given below and in Figure 4.23.

The steps are;

- 0-200s : N₂ (500 sccm)
- 200-400s: CO (500 sccm)
- 400-600s: N₂ (500 sccm)
- 600-800s: CO (500 sccm)
- 800-1000s: N₂ (500 sccm)

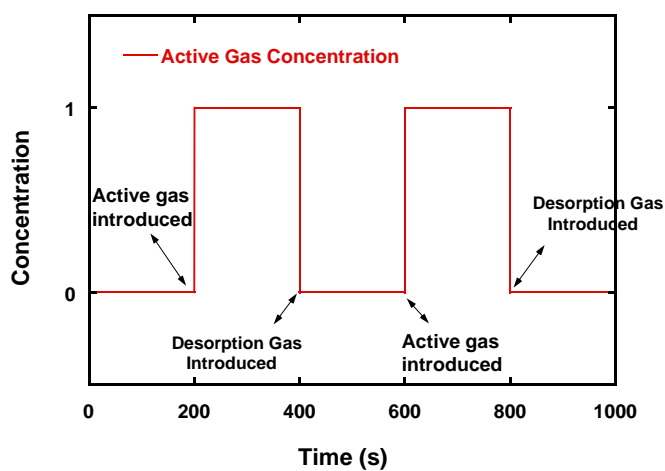


Figure 4.23. Steps of periodic measurement

According to measurements, it was seen that all molecules were insulator. Hence, the electrical properties of any molecules under exposure of CO could not be investigated. The obtained signals were quite noisy. Figure 4.24 shows the electrical signal of calix 8 under exposure of CO for periodic measurement. As seen in Figure 4.24, the resistance was around $10^8\Omega$ and no change in resistance was seen when CO was sent to test cell.

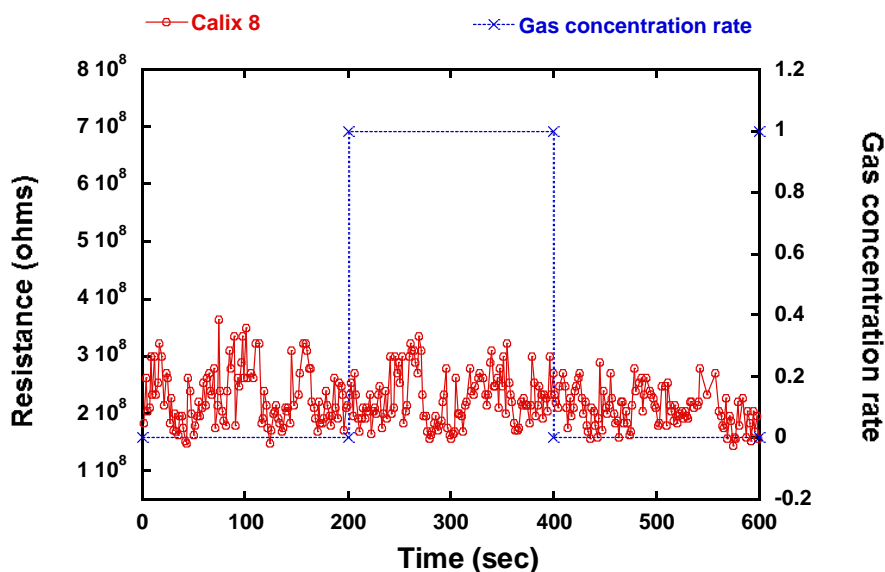


Figure 4.24. Electrical response of Calix 8 under exposure of CO

The electrical properties of iron doped calixarene molecules were also investigated but same results were obtained. However, in order to investigate electrical properties of iron doped calixarene molecules, some carbon nanotube (CNT) were added into each iron doped solution. The aim of adding CNT into each solution was to increase the conductivity of each iron doped calixarene molecule. After adding CNT into calixarene molecule, thin film of each molecule was prepared by using drop-casting technique. Among all prepared thin films, electrical signal from only CNT added iron (III) chloride doped calix 6 could be obtained. The reason why other calixarene molecules showed no response may be due to the fact that CNTs having very small diameter (around 2 nm) are surrounded by non-conductive calixarene molecules giving rise to high resistance. By analysing data (resistance) obtained from measurements, the sensitivity of CNT added iron (III) chloride doped calix 6 was investigated. The sensitivity was given as

$$S = \frac{|R_g - R_0|}{R_0}$$

where R_g and R_0 are the resistivity of the sensor in the gas/ N_2 mixture and in pure N_2 , respectively.

Electrical response and sensitivity of CNT added iron (III) chloride doped calixarene under exposure of CO were given in Figure 4.25 and Figure 4.26, respectively. The initial resistance (resistance of sensor in pure N_2 ; R_0) was measured as 56.62Ω . Here, DC voltage (1V) was applied between electrodes.

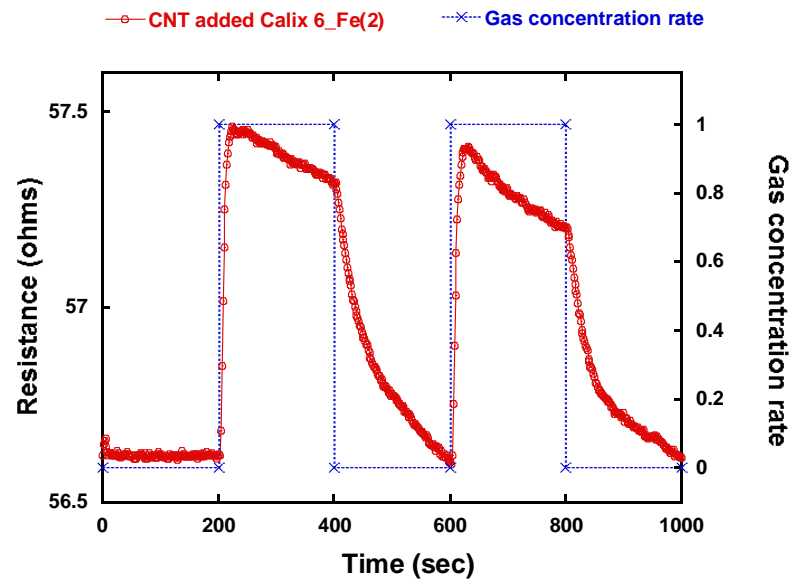


Figure 4.25. Electrical response of CNT added Calix 6_Fe(2)

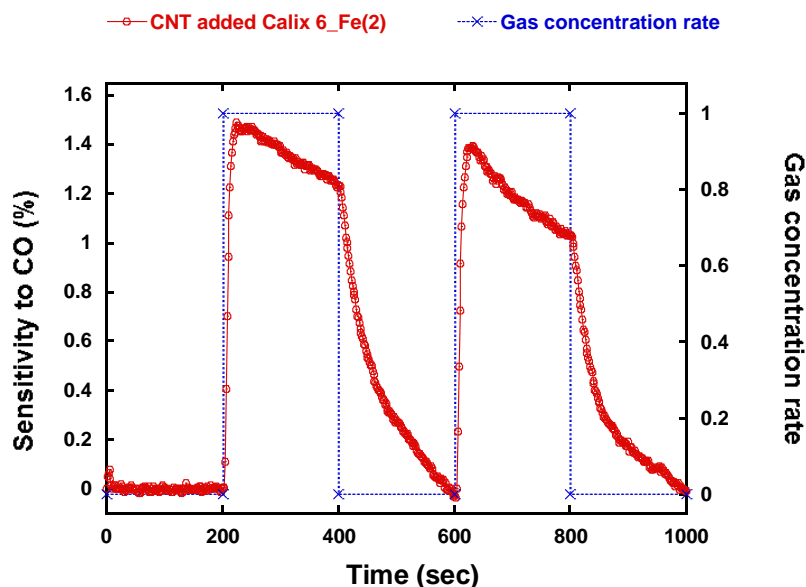


Figure 4.26. Sensitivity of CNT added Calix 6_Fe(2)

The sensor response increases with increasing gas concentration in the gas/N₂ mixture. It is also seen from Figure 4.25 that the resistance increases during adsorption of CO. The conductivity decrease of the CNT containing film coated on IDEs may be resulting from the interaction between CNT's unpaired p_z orbitals which is responsible for electrical conduction of the CNTs with CO's unpaired electrons that provides the interaction mechanism for adsorption. It can be speculated that the weak interaction forces due to CO adsorption on CNTs may decrease the number of available charge carrying electrons and thus yielding a conductivity decrease of the CNTs.

CHAPTER 5

CONCLUSION

This thesis focused on investigation of CO gas adsorption kinetics of various functional calixarene molecules doped with Fe by using quartz crystal microbalance technique. The two different iron compounds, iron (III) nitrate ($\text{Fe}(\text{NO}_3)_3 \cdot 9\text{H}_2\text{O}$) and iron (III) chloride ($\text{FeCl}_3 \cdot 6\text{H}_2\text{O}$), were used to dope calixarene molecules. Five different functional calixarene molecules doped with two different type iron- containing solutions have been used in this thesis study and Calix 1 has been used as reference molecule. Each solution of calixarene molecules has been doped with iron and then thin films of each doped and undoped calixarene molecules on QCM were prepared by utilising drop-casting technique. In order to carry out experiments, a gas measurement system controlling gas flow and concentration for a desired time via computer has been used. The CO gas adsorption kinetics of each QCM electrodes has been investigated.

In Chapter 1, gas sensor literature about CO and its interaction with haemoglobin molecule, with iron content, has been briefly given.

Chapter 2 begins with the introduction of characteristics for an ideal sensor. The different types of sensor with different working principle were explained. Afterwards, piezoelectricity and working principle of quartz crystal microbalance technique were given in details. Finally, the calixarene molecules, used as sensing material, were explained.

Chapter 3 consists of three subtitles with gas flow control and measurement system, and device fabrication procedure that explains fabrication of interdigitated electrode and the last one is iron doping procedure of various functional calixarene molecules. In the experimental setup, the gas flow control and measurement system used to carry out research activities was explained in details. Then, photolithography technique for fabrication of IDE electrodes was given in details. Mask shape and instruments employed in lithography were also presented. Finally, the steps of doping each calixarene molecules with iron molecules were introduced.

In Chapter 4, the experimental results were given in details. The dipole moments and three dimensional structures of calixarene molecules, calculated by Prof. Dr.

Mustafa Kurt from Ahi Evran University, were given. According to these results, calix 17 has highest dipole moment (7.97 D) while calix 6 has lowest (1.55 D). The variations in dipole moments may be due to different functional groups that have different electronegativity. These variations in geometry of calixarenes have a big role in the experimental results.

QCM results used to investigate CO gas sorption capabilities of each doped and undoped calixarene molecule were given. The CO adsorption and desorption kinetics of all molecules have been discussed with different approaches. By using QCM data of all molecules, the sensitivities of bare and iron doped calixarene molecules to CO were investigated. Results showed that functionalising of calixarene molecules with different functional groups increased the affinity towards CO gas compared to calix 1 which does not have any functional group. According to experimental results, calix 6 showed maximum sensitivity to CO (5.16), while calix 18 showed lowest affinity (0.12). This may be because of that calix 6 seems to have three baskets which will give rise to more place for adsorption of CO. The reason why calix 18 showed lowest sensitivity may be because it has hydroxyl and carbonyl groups which have a potential to make hydrogen bond that may bring about unsuitable conformational structure for adsorption of CO.

It was also seen that there has been a remarkable increase in the sensitivity of each calixarene molecule after doping them with iron. That is, there is a remarkable increase in the affinity of calixarene to CO up to 200 times compared to bare calixarene molecules after Fe(1) doping. This must be due to the fact that carbon monoxide has a remarkable affinity for transition metals and it acts as a ligand towards transition metal through the lone pair on the carbon atom. Among iron (III) nitrate (Fe(1)) doped calixarene molecules, calix 6_Fe(1) has highest affinity towards CO (43.38), while calix 8_Fe(1) has lowest (6.57). This may be because calix 6 has more places for iron molecule. Similarly, among iron (III) chloride (Fe(2)) doped calixarene molecules, calix 8_Fe(2) showed highest sensitivity (38.89), while calix 17_Fe(2) showed lowest with 5.76. If the responses of Fe(2) doped calixarenes are compared with Fe(1) doped ones, it is seen that doping calixarenes with Fe(1) made calixarene more sensitive to CO compared to Fe(2) doped calixarenes. This may be because chloride ion (Cl⁻) is bigger than that of nitrate ion (NO₃⁻) in terms of volume and this may cause steric effect. Furthermore, according to experimental results, there has not been any chemical interaction between iron and CO because the results were repeatable which proves that the bound between iron and calixarene is physical (physisorption).

According to experimental results, it has also been seen that the sensitivities of all calixarene molecules changes linearly with CO gas concentration and there is no remarkable difference between sensitivities in air and N₂ environment.

The Langmuir model has also been given in chapter 4 and it was used to investigate adsorption and desorption parameters of all molecules. That is, adsorption and desorption constants (K_a and K_d), relaxation times, maximum mass loaded on thin films of all calixarenes have been found and given in this chapter.

According to electrical measurements, it is seen that both bare calixarene molecules and iron doped calixarene molecules are non-conductive materials and their resistances are around $10^8\Omega$. Hence, the signals coming from thin films of these molecules coated on IDEs were quite noisy. After adding CNT into iron doped calixarene molecule to increase conductivity, we could obtain signal from iron (III) chloride doped calix 6. The increase in resistivity of the CNT containing film coated on IDEs may stem from the interaction between CNT's unpaired p_z orbitals which is responsible for electrical conduction of the CNTs with CO's unpaired electrons that provides the interaction mechanism for adsorption. It may be thought that the weak interaction forces during adsorption of CO on CNTs may decrease the number of available charge carrying electrons and thus yielding a conductivity decrease of the CNTs. Electrical signals from other molecules were noisy which may be because CNTs having very small diameter (around 2 nm) are surrounded by non-conductive calixarene molecules giving rise to high resistance.

To summarise, the effect of iron doping on the CO gas sensing properties of various functional calixarene molecules was investigated. According to experimental results, doping calixarene molecules with iron increased the affinity of each molecule to CO compared to bare calixarene molecules. Hence, these molecules doped with iron can be utilized as a suitable material in carbon monoxide gas sensor applications.

REFERENCES

- AnthonyáMcKervey, M. 1992. Selective alkali-metal cation complexation by chemically modified calixarenes. Part 4. Effect of substituent variation on the Na⁺/K⁺ selectivity in the ester series and X-ray crystal structure of the trifluoroethyl ester. *Journal of the Chemical Society, Perkin Transactions* 2:1119-1125.
- Arnaudneu, F., E.M. Collins, M. Deasy, G. Ferguson, S.J. Harris, B. Kaitner, A.J. Lough, M.A. Mckervey, E. Marques, B.L. Ruhl, M.J. Schwingweill, and E.M. Seward. 1989. Synthesis, X-Ray Crystal-Structures, and Cation-Binding Properties of Alkyl Calixaryl Esters and Ketones, a New Family of Macrocyclic Molecular Receptors. *J Am Chem Soc.* 111:8681-8691.
- Baekeland, L. 1909. The Synthesis, Constitution, and Uses of Bakelite. *Industrial & Engineering Chemistry.* 1:149-161.
- Bender, M.L., and M. Komiyama. 1978. Cyclodextrin chemistry. Springer-Verlag Berlin.
- Bocchi, V., D. Foina, A. Pochini, R. Ungaro, and G.D. Andreetti. 1982. Synthesis, H-1-Nmr, C-13 Nmr-Spectra and Conformational Preference of Open-Chain Ligands on Lipophilic Macrocycles. *Tetrahedron.* 38:373-378.
- Bochenkov, V., and G. Sergeev. 2010. Sensitivity, Selectivity, and Stability of Gas-Sensitive Metal-Oxide Nanostructures. *Metal Oxide Nanostructures and Their Applications:*31-52.
- Bottom, V.E. 1982. Introduction to quartz crystal unit design. Van Nostrand Reinhold New York.
- Buck, R.P., E. Lindner, W. Kutner, and G. Inzelt. 2004. Piezoelectric chemical sensors - (IUPAC Technical Report). *Pure Appl Chem.* 76:1139-1160.
- Buie, N.M., V.S. Talanov, R.J. Butcher, and G.G. Talanova. 2008. New fluorogenic dansyl-containing calix[4]arene in the partial cone conformation for highly sensitive and selective recognition of lead(II). *Inorg Chem.* 47:3549-3558.
- Burke, A., E. Yilmaz, and N. Hasirci. 2000. Evaluation of chitosan as a potential medical iron (III) ion adsorbent. *Turkish Journal of Medical Sciences.* 30:341-348.
- Capone, S., A. Forleo, L. Francioso, R. Rella, P. Siciliano, J. Spadavecchia, D.S. Presicce, and A.M. Taurino. 2003. Solid state gas sensors: State of the art and future activities. *J Optoelectron Adv M.* 5:1335-1348.
- Chang, S.K., S.K. Kwon, and I. Cho. 1987. Calixarene-Based Amide Ionophores for Group-Iia Metal-Cations. *Chem Lett:*947-948.

- Chen, L.X., X.W. He, B.T. Zhao, and Y. Liu. 2000. Calixarene derivative as the neutral carrier in silver ion-selective electrode and liquid membrane transport. *Anal Chim Acta*. 417:51-56.
- Choi, J.D., and G.M. Choi. 2000. Electrical and CO gas sensing properties of layered ZnO-CuO sensor. *Sensor Actuat B-Chem*. 69:120-126.
- Chou, J. 2000. Hazardous gas monitors: a practical guide to selection, operation and applications. McGraw-Hill.
- Demendoza, J., P. Prados, N. Campillo, P.M. Nieto, C. Saez, J.P. Fayet, M.C. Vertut, C. Jaime, and J. Elguero. 1993. Dipole-Moments Can Be Used to Determine the Conformation of Calix[4]Arenes. *Recl Trav Chim Pay B*. 112:367-369.
- Demirel, N., M. Merdivan, N. Pirinccioglu, and C. Hamamci. 2003. Thorium(IV) and uranium(VI) sorption studies on octacarboxymethyl-C-methylcalix[4]resorcinarene impregnated on a polymeric support. *Anal Chim Acta*. 485:213-219.
- Ebersole, R.C., J.A. Miller, J.R. Moran, and M.D. Ward. 1990. Spontaneously Formed Functionally Active Avidin Monolayers on Metal-Surfaces - a Strategy for Immobilizing Biological Reagents and Design of Piezoelectric Biosensors. *J Am Chem Soc*. 112:3239-3241.
- Ferguson, G., B. Kaitner, M.A. Mckerverey, and E.M. Seward. 1987. Synthesis, X-Ray Crystal-Structure, and Cation Transfer Properties of a Calix[4]Arene Tetraketone, a New Versatile Molecular Receptor. *J Chem Soc Chem Comm*:584-585.
- Fileenko, D., T. Gotszalk, Z. Kazantseva, O. Rabinovych, I. Koshets, Y. Shirshov, V. Kalchenko, and I.W. Rangelow. 2005. Chemical gas sensors based on calixarene-coated discontinuous gold films. *Sensor Actuat B-Chem*. 111:264-270.
- Goldstein, M. 2008. Carbon Monoxide Poisoning. *Journal of emergency nursing: JEN : official publication of the Emergency Department Nurses Association*. 34:538-542.
- Gründler, P. 2007. Chemical sensors: an introduction for scientists and engineers. Springer.
- Guinier, A., and J. Remi. 1989. The solid state.
- Gupta, A., and S.M. Khopkar. 1995. Solvent-Extraction Separation of Cobalt(II) with Hexaacetatocalix(6)Arene. *Talanta*. 42:1493-1496.
- Gutsche, C., and J. Stoddart. 1989. Calixarenes: monographs in supramolecular chemistry. by JF Stoddart, the Royal Society of Chemistry, Cambridge. 1.

- Gutsche, C.D., B. Dhawan, J.A. Levine, K.H. No, and L.J. Bauer. 1983. Calixarenes-9 - Conformational Isomers of the Ethers and Esters of Calix[4]Arenes. *Tetrahedron*. 39:409-426.
- Gutsche, C.D., and M. Iqbal. 1990. Para-Tert-Butylcalix[4]Arene. *Org Synth*. 68:234-237.
- Gutsche, C.D., and R. Muthukrishnan. 1978. Calixarenes. 1. Analysis of the product mixtures produced by the base-catalyzed condensation of formaldehyde with para-substituted phenols. *The Journal of Organic Chemistry*. 43:4905-4906.
- Gutsche, C.D., and K.C. Nam. 1988. Calixarenes. 22. Synthesis, properties, and metal complexation of aminocalixarenes. *J Am Chem Soc*. 110:6153-6162.
- Hess, P. 2002. Surface acoustic waves in materials science. *Phys Today*. 55:42-47.
- Hook, J.R., and H.E. Hall. 2000. Solid State Physics (The Manchester Physics Series). John Wiley and Sons Ltd.
- Hulanicki, A., S. Glab, and F. Ingman. 1991. Chemical Sensors Definitions and Classification. *Pure Appl Chem*. 63:1247-1250.
- Izatt, R.M., J.S. Bradshaw, K. Pawlak, R.L. Bruening, and B.J. Tarbet. 1992. Thermodynamic and kinetic data for macrocycle interaction with neutral molecules. *Chemical reviews*. 92:1261-1354.
- Janshoff, A., H.J. Galla, and C. Steinem. 2000. Piezoelectric mass-sensing devices as biosensors - An alternative to optical biosensors? *Angew Chem Int Edit*. 39:4004-4032.
- Kalchenko, V., I. Koshets, E. Matsas, O. Kopylov, A. Solovyov, Z. Kazantseva, and Y.M. Shirshov. 2002. Calixarene based QCM sensors array and its response to volatile organic vapors. *Materials Science*. 20:73-88.
- Kanazawa, K.K., and J.G. Gordon. 1985. Frequency of a quartz microbalance in contact with liquid. *Anal Chem*. 57:1770-1771.
- Karpovich, D.S., and G.J. Blanchard. 1994. Direct Measurement of the Adsorption-Kinetics of Alkanethiolate Self-Assembled Monolayers on a Microcrystalline Gold Surface. *Langmuir*. 10:3315-3322.
- Katsu, T., Y. Yokoyama, K. Ueda, K. Kohno, and T. Yamato. 2005. Potassium-selective membrane electrodes based on macrocyclic metacyclophanes analogous to calixarenes. *Anal Sci*. 21:175-178.
- Kelderman, E., L. Derhaeg, G.J.T. Heesink, W. Verboom, J.F.J. Engbersen, N.F. Vanhulst, A. Persoons, and D.N. Reinhoudt. 1992. Nitrocalix[4]Arenes as Molecules for 2nd-Order Nonlinear Optics. *Angew Chem Int Edit*. 31:1075-1077.

- Khatko, V., E. Llobet, X. Vilanova, J. Brezmes, J. Hubalek, K. Malysz, and X. Correig. 2005. Gas sensing properties of nanoparticle indium-doped WO₃ thick films. *Sensor Actuat B-Chem.* 111:45-51.
- Kim, S.-y., and K. No. 2007. Synthesis of calixsalen: A route to azacalixarene analogue. *BULLETIN-KOREAN CHEMICAL SOCIETY.* 28:315.
- Kimura, K., T. Miura, M. Matsuo, and T. Shono. 1990. Polymeric Membrane Sodium-Selective Electrodes Based on Lipophilic Calix[4]Arene Derivatives. *Anal Chem.* 62:1510-1513.
- Kirschner, J. Surface Acoustic Wave Sensors (SAWS).
- Kocabas, E., A. Karakucuk, A. Sirit, and M. Yilmaz. 2006. Synthesis of new chiral calix[4]arene diamide derivatives for liquid phase extraction of alpha-amino acid methylesters. *Tetrahedron-Asymmetr.* 17:1514-1520.
- Koshets, I.A., Z.I. Kazantseva, Y.M. Shirshov, S.A. Cherenok, and V.I. Kalchenko. 2005. Calixarene films as sensitive coatings for QCM-based gas sensors. *Sensor Actuat B-Chem.* 106:177-181.
- Lehn, J.M. 1988. Supramolecular chemistry—scope and perspectives molecules, supermolecules, and molecular devices (Nobel Lecture). *Angewandte Chemie International Edition in English.* 27:89-112.
- Ma, Q.L., H.M. Ma, M.H. Su, Z.H. Wang, L.H. Nie, and S.C. Liang. 2001. Determination of nickel by a new chromogenic azocalix[4]arene. *Anal Chim Acta.* 439:73-79.
- Madou, M.J. 2002. Fundamentals of microfabrication: the science of miniaturization. CRC Press LLC.
- MALKHEDE, D.D., P.M. DHADKE, and S.M. KHOPKAR. 1999. Solvent-Extraction Separation of Manganese (II) with Calixarene Substituted with an Acetyl Group at the Lower Rim. *Anal Sci.* 15:781-784.
- Myers, H. 1997. Introductory Solid State Physics, Taylor & Francis. London.
- Nawara, K., J. McCracken, P.G. Kryszinski, and G.J. Blanchard. 2013. Structure-Dependent Complexation of Fe³⁺ by Anthracyclines. 1. The Importance of Pendant Hydroxyl Functionality. *The Journal of Physical Chemistry B.*
- Ochiai, B., M. Kamiya, and T. Endo. 2012. Synthesis and Fe(III)-complexation ability of polyurethane bearing kojic acid skeleton in the main chain prepared by polyaddition of aliphatic hydroxyl groups without protection of phenolic hydroxyl groups. *J Polym Sci Pol Chem.* 50:3493-3498.
- Ohira, S.I., E. Wanigasekar, D.M. Rudkevich, and P.K. Dasgupta. 2009. Sensing parts per million levels of gaseous NO₂ by a optical fiber transducer based on calix[4]arenes. *Talanta.* 77:1814-1820.

- Okur, S., M. Kus, F. Ozel, and M. Yilmaz. 2010. Humidity adsorption kinetics of water soluble calix[4]arene derivatives measured using QCM technique. *Sensor Actuat B-Chem.* 145:93-97.
- Pedersen, C.J. 1967. Cyclic polyethers and their complexes with metal salts. *J Am Chem Soc.* 89:7017-7036.
- Raub, J.A., M. Mathieu-Nolf, N.B. Hampson, and S.R. Thom. 2000. Carbon monoxide poisoning - a public health perspective. *Toxicology.* 145:1-14.
- Richardson, T., R. Brook, F. Davis, and C. Hunter. 2006a. The NO₂ gas sensing properties of calixarene/porphyrin mixed LB films. *Colloids and Surfaces A: Physicochemical and Engineering Aspects.* 284:320-325.
- Richardson, T.H., R.A. Brook, F. Davis, and C.A. Hunter. 2006b. The NO₂ gas sensing properties of calixarene/porphyrin mixed LB films. *Colloid Surface A.* 284:320-325.
- Rodkey, F.L., J.D. O'Neal, H.A. Collison, and D.E. Uddin. 1974. Relative affinity of hemoglobin S and hemoglobin A for carbon monoxide and oxygen. *Clinical chemistry.* 20:83-84.
- Sauerbrey, G. 1959. Use of quartz vibration for weighing thin films on a microbalance. *J. Physik.* 155:206-212.
- Sayin, S., G.U. Akkus, R. Cibulka, I. Stibor, and M. Yilmaz. 2011. Synthesis of Flavin-Calix[4]arene Conjugate Derivatives. *Helv Chim Acta.* 94:481-486.
- Sayin, S., F. Ozcan, and M. Yilmaz. 2010. Synthesis and evaluation of chromate and arsenate anions extraction ability of a N-methylglucamine derivative of calix[4]arene immobilized onto magnetic nanoparticles. *J Hazard Mater.* 178:312-319.
- Sayin, S., and M. Yilmaz. 2011. Synthesis of a new calixarene derivative and its immobilization onto magnetic nanoparticle surfaces for excellent extractants toward Cr (VI), As (V), and U (VI). *Journal of Chemical & Engineering Data.* 56:2020-2029.
- Struttmann, T., A. Scheerer, T.S. Prince, and L.A. Goldstein. 1998. Unintentional carbon monoxide poisoning from an unlikely source. *J Am Board Fam Pract.* 11:481-484.
- Szejtli, J. 1988. Cyclodextrin technology. Springer.
- Talanova, G.G., N.S.A. Elkarim, V.S. Talanov, and R.A. Bartsch. 1999. A calixarene-based fluorogenic reagent for selective mercury(II) recognition. *Anal Chem.* 71:3106-3109.

- Talanova, G.G., E.D. Roper, N.M. Buie, M.G. Gorbunova, R.A. Bartsch, and V.S. Talanov. 2005. Novel fluorogenic calix[4] arene-bis(crown-6-ether) for selective recognition of thallium(I). *Chem Commun*:5673-5675.
- von Baeyer, A. 1872. Ber., 1872, 5, 25.(b) von Baeyer, Ber., 1872, 5, 280.(c) von Baeyer, A. Ber.
- Yoon, D.H., and G.M. Choi. 1997. Microstructure and CO gas sensing properties of porous ZnO produced by starch addition. *Sensor Actuat B-Chem.* 45:251-257.
- Yuan-Yuan, L., Y. Hong-Zong, H. Xi-Wen, C. Lang-Xing, Z. Guo-Zhu, and H. Jia-Qi. 2005. QCM Coated with Self-assembled Cystine-bearing 1, 3-Bridged Calix [4] arenes for Recognizing Gas-phase Butylamines. *Chinese Journal of Chemistry.* 23:571-575.
- Zhang, S.H., and W.S. Huang. 2001. Simultaneous determination of Cd²⁺ and Pb²⁺ using a chemically modified electrode. *Anal Sci.* 17:983-985.
- Zheng, Y.S., and C. Zhang. 2004. Exceptional chiral recognition of racemic carboxylic acids by calix[4]arenes bearing optically pure (alpha,ss-amino alcohol groups). *Org Lett.* 6:1189-1192.
- Zheng, Y.S., C. Zhang, Z.F. Tian, and A. Jiang. 2004. Synthesis of nitrogen-containing chiral calix[4]arene crown and semi-crown ether. *Synthetic Commun.* 34:679-688.
- Zinke, A., and E. Ziegler. 1944. Zur Kenntnis des Härtungsprozesses von Phenol-Formaldehyd-Harzen, X. Mitteilung. *Berichte der deutschen chemischen Gesellschaft (A and B Series).* 77:264-272.